The lateritic profile of Balkouin, Burkina Faso: geochemistry, mineralogy and genesis

The lateritic profile of Balkouin, Burkina Faso: geochemistry, mineralogy and genesis

Ilaria Giorgis[a], Sabrina Bonetto[a], Roberto Giustetto[a], Abdou Lawane[b], Anne Pantet[c] Piergiorgio Rossetti[a]*, Jean-Hugues Thomassin[d], Raffaele Vinai[b]

[a] Department of Earth Sciences, University of Turin, via Valperga Caluso 35, I-10125 Turin, Italy
[b] Laboratoire Eco-Matériaux et Techniques de Constructions (LEMC), 2iE, 01 BP 594 Ouagadougou 01, rue de la Science, Burkina Faso
[c] LOMC-CNRS, University of Havre, UMR 6294 Havre, France
[d] ENSIP, University of Poitiers, 1 rue Marcel Doré, bat B1, 86022 Poitiers Cedex, France

*corresponding author:

Piergiorgio Rossetti
Department of Earth Sciences
University of Turin
via Valperga Caluso 35
I-10125 Turin, Italy

E-mail address: piergiorgio.rossetti@unito.it
Tel.: +39 011 6705174
Fax: +39 011 6705128

Abstract

This study reports on the geochemical and mineralogical characterization of a lateritic profile cropping out in the Balkouin area, Central Burkina Faso, aimed at obtaining a better understanding of the processes responsible for the formation of the laterite itself and the constraints to its development. The lateritic profile rests on a Paleoproterozoic basement mostly composed of granodioritic rocks related to the Eburnean magmatic cycle passing upwards to saprolite and consists of four main composite horizons (bottom to top): kaolinite and clay-rich horizons, mottled laterite and iron-rich duricrust. In order to achieve such a goal, a multi-disciplinary analytical approach was adopted, which includes inductively coupled plasma (ICP) atomic emission and mass spectrometries (ICP-AES and ICP-MS respectively), X-ray powder diffraction (XRPD), scanning electron microscopy with energy dispersive spectrometry (SEM-EDS) and micro-Raman spectroscopy.

The geochemical data, and particularly the immobile elements distribution and REE patterns, show that the Balkouin laterite is the product of an *in situ* lateritization process that involved a strong depletion of the more soluble elements (K, Mg, Ca, Na, Rb, Sr and Ba) and an enrichment in Fe; Si was also removed, particularly in the uppermost horizons. All along the profile the change in composition is coupled with important changes in mineralogy. In particular, the saprolite is characterized by occurrence of abundant albitic plagioclase, quartz and nontronite; kaolinite is apparently absent. The transition to the overlying lateritic profile marks the breakdown of plagioclase and nontronite, thus allowing kaolinite to become one of the major components upwards, together with goethite and quartz. The upper part of the profile is strongly enriched in hematite (+ kaolinite). Ti oxides (at least in part as anatase) and apatite are typical accessory phases, while free aluminum hydroxides are notably absent. Mass change calculations emphasize the extent of the mass loss, which exceeds 50 wt% (and often 70 wt%) for almost all horizons; only Fe was significantly concentrated in the residual system.

The geochemical and mineralogical features suggest that the lateritic profile is the product of a continuous process that gradually developed from the bedrock upwards, in agreement with the Schellmann classic genetic model. The laterite formation must have occurred at low pH ($\leq$ 4.5) and high Eh ($\geq$ 0.4) values, i.e., under acidic and oxidizing environments, which allowed strongly selective leaching conditions. The lack of gibbsite and bohemite is in agreement with the compositional data: the occurrence of quartz (± amorphous silica) all along the profile was an inhibiting factor for the formation of free aluminum hydroxides.

Keywords:
selective leaching processes, whole rock geochemistry, REE, powder XRPD, Rietveld method, SEM-EDS analyses, micro-Raman, mass change, Eh-pH

1. Introduction

More than 200 years ago Francis Buchanan, a surgeon travelling in southern India, coined the term laterite (from the Latin *later-eris*, i.e., brick) to describe "*an indurated clay*" which "*is one of the most valuable materials for building. It is diffused in immense masses… and is placed over the granite…. It contains a very large quantity of iron in the form of yellow and red ochres…*" (Buchanan, 1807, pp. 440-441). Since then, the term "laterite" has been widely used for describing a rock deriving from extreme superficial weathering, generally under tropical climatic conditions. As assessed by abundant studies, the severe weathering conditions of tropical regions trigger strong transformations – involving selective leaching processes - leading to the formation of "lateritic rocks". These rocks are often used as building materials but can also be exploited for other types of mineral resources (e.g., Al, Ni, Fe, Au: Robb, 2005, and refs. therein). As pointed out by Eggleton and Taylor (1999), Buchanan's original definition was actually abandoned and the term "laterite" is nowadays used by different authors with different meanings, indicating a specific material (i.e., as a rock term) or a group of materials organized in a particular way (i.e., "lateritic profile"), often with a genetic connotation.

An important attempt to re-define laterite was done about 30 years ago by Schellmann (1983, 1986), who proposed a new definition and classification based on rock chemistry - namely, on the Si/(Al+Fe) ratio - in comparison to the chemical composition of the underlying parent rock. Though widely used, such an approach was strongly criticized by several authors (e.g., Bourman and Ollier, 2002, 2003; reply in Schellmann, 2003), who proposed that the term "laterite" should have been abandoned. Such a term, however, is so widely used nowadays that its abandonment seems at least unrealistic. The "laterite problem" is largely based on the fact that when studied in detail (e.g., Dahanayake, 1982; Théveniaut and Freyssinet, 1999; Hieronymous et al., 2001; Kasthurba et al., 2005, 2007; Ollier and Sheth, 2008; Fernández-Caliani and Cantano, 2010), in spite of apparent similarities each lateritic profile is unique because of its development depending on several factors, such as climate, morphology, bedrock composition, hydrogeology etc. The in-depth understanding of the lateritic materials needs therefore detailed multidisciplinary studies, which involve both field and laboratory investigations (Bourman, 1993).

To achieve a better understanding of the multiple processes involved in laterite formation and the eventual constraints limiting its development, a detailed geological, mineralogical and geochemical characterization of a lateritic profile cropping out in the Balkouin area, Central Burkina Faso (Giorgis, 2012), was performed. The investigated profile rests on a Paleoproterozoic basement mostly composed of granodioritic rocks, related to the Eburnean magmatic cycle, passing upwards to saprolite and consisting of four composite levels, including (bottom to top) kaolinite and clay-rich horizons, mottled laterite and iron-rich duricrust. The study, conducted *via* an in-depth, multidisciplinary analytical approach, is part of a project coordinated by LEMC (Laboratoire d'Eco-Matériaux de Construction) of the Institut International d'Ingénierie de l'Eau et de l'Environnement (2iE), whose purpose is the contribution to the development of eco-sustainable materials - including laterite as a building material (Lawane et al., 2011). Several studies were performed in Western and Central Africa, focused on the geotechnical and mechanical characteristics of the lateritic *soils* (or "lateritic gravels") and their possible use in the construction of roads and trails, especially in Ghana (Gidigasu, 1971, 1974, with refs.) and more recently in Burkina Faso (Millogo et al., 2008). Studies focused, instead, on lateritic *rocks*, aimed at developing a standard for their use for building purposes, were performed recently, particularly in India (Kasthurba et al., 2005, 2007). In spite of their widespread diffusion, these rocks did not apparently receive so far great attention, especially in Western and Central Africa, and only recently some projects started in order to possibly valorize them as potential building materials (Lawane et al., 2011; Lecomte-nana et al., 2009). Within the circles of the above mentioned project, the data presented in this paper will hopefully also contribute to understand the influence of the chemical and mineralogical features of laterite on its engineering properties.

2. Geological setting and climate

2.1. Regional geology

Burkina Faso is mainly composed of precambrian rock sequences belonging to the West-African craton, made of a Paleoproterozoic basement and its sedimentary covers (Sattran and Wenmenga, 2002; Castaing et al., 2003a and refs. therein). The basement is characterized by the occurrence of the Birimian greenstone belts (2238-2170 Ma: Castaing et al., 2003a), volcano-sedimentary and plutonic sequences mostly oriented NNE-SSW, affected by a greenschist to (locally) amphibolite facies metamorphic overprint. The greenstone belts are intruded by abundant acidic magmatic bodies (Eburnean magmatism), that have been divided into a tonalite (2210-2100 Ma) and a generally younger granite suite (2150-1819 Ma: Castaing et al., 2003a). The basement is unconformably covered by a Neoproterozoic to Lower Paleozoic sequence in the far West and South-East of the country, as part of the Taoudenni and Volta sedimentary basins respectively. Some terrigenous formations of Cenozoic age also occur in the far North-West and East areas (Sattran and Wenmenga, 2002).

Most of the country is covered by a relatively flat peneplain, which forms a gently undulating landscape. Isolated hills are generally rests of Precambrian massifs, apart from the steeply-sided Paleozoic sandstone massif where the Tena Kourou peak (749 m) stands.

2.2. Geology of the Balkouin area

The Balkouin village is located in Central Burkina Faso, ca. 20 km South-East of the capital Ouagadougou (Fig. 1), at a height of 304 m a.s.l. This area is mainly composed of Paleoproterozoic acidic to intermediate magmatic rocks belonging to the Birimian basement, related to the Eburnean magmatic cycle. They are represented by different varieties of granitic rocks (biotite ± amphibole medium-grained granite; biotite + amphibole porphyritic granodiorite; biotite ± muscovite medium-fine grained granite), which intrude bodies of locally foliated granodiorite, tonalite and quartz-diorite (“tonalitic suite”), dated at 2140±6 Ma (Castaing et al., 2003a, b). Remnants of older volcano-sedimentary and plutonic formations, metamorphosed by the Eburnean event, are represented by scattered bodies of amphibole gneiss (one cropping out at Balkouin according to Castaing et al., 2003b; Fig. 1), volcano-sedimentary schists and rhyolitic rocks within the granites. Rocks belonging to a “leptynite-granodiorite complex” also crop out in the South-East. The Birimian basement is crosscut by WNW-ESE trending dolerite dykes and affected by minor fracture/fault systems, mostly oriented NE-SW (Fig. 1).

FIG_1

As in most of the country, the basement outcrops are relatively rare. In fact, the peneplain developed on the Paleoproterozoic basement is covered by a 5 to 15 m thick blanket of laterite, which is often mined as a building material. Only locally the basement is visible, in the form of rounded outcrops surrounded by a residual laterite mantle.

2.3. Climate and drainage conditions

Burkina Faso is classified as an intertropical country displaying a strong Sudano-Sahelian climate (Sattran and Wenmenga, 2002). The alternation, all year round, of dry and wet seasons whose length varies from South to North allows the distinction of three climatic zones: i) the South-Western (wettest) Sudanese zone; ii) the Northern (driest) Sahelian zone and iii) the Sudano-Sahelian zone, in the central part of the country, which shows intermediate characters. About 40 years ago the limits among different zones started to move southwards as a consequence of climate changes.

The study area falls within the central Sudano-Sahelian zone, where the pluviometric values range between 900 and 600 mm, the dry season lasts from October to May with average monthly temperatures ranging from 13°C to 40°C. The average annual conditions for the Balkouin area are 28.8°C and 897 mm of rainfall (Sattran and Wenmenga, 2002).

Even if relatively flat (most of the country lies at heights comprised between 250 and 300 m a.s.l.), Burkina Faso shows an important hydrographic network mostly composed of sub-basins of the Volta River system (Mouhoun River, former Black Volta; Nakambé River, former White Volta; Nazinon River, former Red Volta), which flow in Ghana to form the Volta River and Lake. The Balkouin area lies within a site drained by creeks flowing to the east, which belongs to the sub-basin of the Nakambé river. Such an area belongs to the huge peneplain developed over the eroded Birimian Paleoproterozoic basement.

The climate conditions (tropical climate with an average temperature exceeding 18°C; abundant precipitations exceeding evaporation) and geological framework (particular tectonic stability since the Tertiary Era and consequent flat morphology) favoured the development of a semi-continuous lateritic cover, probably starting from the Cretaceous on (Hottin and Ouedraogo, 1975).

2.4. The Balkouin lateritic profile

Outcrops displaying a complete lateritic profile are rarely observed in Burkina Faso. This is valid also in the Balkouin area, where a complete section cannot be observed in a single locality. A careful mapping of the area around the Balkouin village, within laterite quarries and along scattered outcrops and trenches, however, allowed a complete reconstruction of the whole lateritic profile, from the underlying bedrock to the Fe-rich duricrust (Fig. 2, Plate 1; labels refer to the studied samples).

PLATE_1

FIG_2

The *bedrock* is exposed in few outcrops occurring along the roads around Balkouin, within trenches excavated for quarrying activities and/or as rounded, denudated exposures. Two dominant rock-types were identified in the area:

- medium- to fine-grained biotite ± amphibole granite/granodiorite (sample BVIIa), locally porphyritic and sometimes crosscut by decimetre-thick aplite and/or pegmatite dykes (Plate 1a). It represents the most common rock-type of the basement;
- fine-grained foliated granodiorite (BVIIb), composed of a fine-grained quartz-feldspatic matrix containing mm-sized black amphibole. Such a rock-type probably corresponds to the amphibole gneiss mentioned by Castaing et al. (2003a, b; see Fig. 1).

The bedrock passes upwards to saprolite (BVI, Plate 1b; possibly few decimetres to 2 m thick), which is observed only in few scattered outcrops and occurs as a highly brittle but still coherent white-yellowish to light-brown rock. This saprolite, related by definition to the isovolumetric weathering of the underlying rock, shows a microgranular texture made of mm-sized feldspar, quartz and scarce altered mafic phases which still allow the recognition of a magmatic protolith.

The overlying lateritic profile, around 10 m thick, is composed of (bottom to top):

1 - *Kaolinite horizon*, composed of:
a) kaolinitic, highly friable laterite (BVb, Plate 1c; ≤1 m thick), generally white in colour with minor white-reddish irregular patches;
b) light red laterite (BVa, Plate 1d; ≤1 m thick), made of irregularly alternating light red to white domains. It contains mm- to cm-sized quartz clasts.

2 - *Clay-rich horizon* (≤2 m thick), including:

a) very fine-grained, clay-rich laterite (BIVb, Plate 1e; 0.7-1m thick), ochre-coloured and strongly homogeneous as a rule, with the exception of local yellowish, kaolinite-rich cm-sized portions;
b) "chaotic laterite" (BIVa, Plate 1e; 0.5-1 m thick), made of mm- to cm-sized yellowish to brownish-black "clasts" embedded in a fine-grained ochre matrix. Fragments of quartz veins also occur.

3 - *Mottled horizon* (Plate 1f-i; 3-5 m thick). It is softer than the overlying ones and composed of irregularly alternating reddish and yellowish cm-sized portions. It consists of two separate portions:
a) poorly coherent laterite (BIIIb, Plate 1f; 1 m thick), composed of a reddish matrix embedding white-yellowish, often elongated kaolinite-rich domains, passing upwards to strongly brittle, light reddish to whitish laterite (BIIIa, Plate 1g; ca. 1m thick);
b) reddish brittle laterite (BIIa, b, c, Plate 1h, i; 2-3 m thick) made of a reddish, often vacuolar matrix embedding cm-sized yellowish to whitish domains. Samples BIIa and BIIb were collected within a quarry where this rock is exploited as a building material (Plate 1h).

4 - *Fe-rich duricrust horizon*, made of:
a) reddish, strongly indurated laterite (BIb; 80 cm thick) displaying a poorly developed pisolitic texture. It occasionally contains mm- to cm-sized irregularly shaped whitish to yellowish portions (much less abundant, however, than in the underlying horizons) and locally passes to ochre-colored, vermicular anastomosed laterite;
b) upper reddish to dark brown, strongly indurated laterite (sample BIa, that cannot be cut with the traditional methods), ca. 70 cm thick, with well developed pisolitic texture ("*pisolitic laterite*", Plate 1l).

3. Materials and methods

Several analytical techniques, whose details are aptly summarized in Table 1, were applied in order to adequately characterize the different horizons representative of the lateritic profile described above. Technical data and specifications for each analytical technique are exhaustively detailed in the Appendix.

TABLE 1

Geochemical analyses:
a) Whole rock analyses. Inductively coupled plasma (ICP) atomic emission spectrometry (AES) and mass spectrometry (MS) were performed for major elements and trace/rare earth elements (REE) respectively, in order to obtain the bulk composition for all lateritic horizons, underlying saprolite and basement rocks.
b) Spot analyses. Scanning electron microscopy (SEM) – energy dispersive spectrometry (EDS) analyses (spot diameter:1-2 μm) were collected directly on broken rock chips, in order to acquire information about the composition of mineral phases, especially the minor ones possibly overlooked by other techniques (i.e. X-ray powder diffraction – see below).

Mineralogical analyses:
a) Whole rock analyses. X-ray powder diffraction (XRPD) techniques were performed on laterite specimens extracted from all described horizons and preliminarily crushed in an agate mortar, in order to identify the main mineral components both qualitatively and quantitatively.

b) Localized analyses. Micro-Raman data were collected on selected samples so to possibly characterize minor and/or accessory phases and further confirm the mineralogical composition of the different lateritic horizons. This spectroscopic technique, allowing *in situ* data acquisition from very small rock volumes (few to some tens of μm^3, depending on the adopted laser wavelength and magnification) with no preliminary treatment, often allows an unambiguous recognition of mineral phases hard to trace with XRPD and/or SEM-EDS due to their low abundance and/or particular chemistry (e.g., TiO_2 polymorphs; hematite/goethite, etc.).

4. Results

4.1. Geochemical features of the lateritic profile

Whole rock analyses of specimens extracted throughout all the lateritic profile (from the basement rocks to the iron-rich duricrust) are given in Table 2. The variations affecting the distribution of selected major and trace elements along the profile are shown in Fig. 3. In Fig. 4 data are plotted in the Al_2O_3-SiO_2-Fe_2O_3 ternary diagram, adopted by Schellmann (1983, 1986) and widely used to describe the lateritic rocks composition. Variation diagrams of selected elements against TiO_2 are shown in Fig. 5, while chondrite- and bedrock-normalized REE patterns are shown in Figs. 6 and 7, respectively.

TABLE_2

FIG. 3

4.1.1. Major elements

Two bedrock samples have been analyzed: a medium-grained biotite ± amphibole granodiorite (BVIIa) and a fine-grained foliated granodiorite (BVIIb; Table 2). Both these specimens show an almost identical chemistry and can be classified, based on their normative composition, as quartz-poor granodiorites. The overall chemical composition, and particularly the high Na_2O content (~5.5 wt%) coupled with the relatively low MgO, K_2O and CaO values, suggests that these intrusive rocks, probably related to the same magmatic event (as strongly suggested by the REE data: see below), may have been affected by albitization processes. If compared to the basement rocks, all the overlying horizons show a marked increase in the water content: the LOI values, which reach less than 1 wt % in the fresh rocks, sharply pass to more than 7 wt % in the saprolite and become > 9 wt% in almost all laterite horizons.

In spite of its partly preserved mesoscopic structure, the composition of saprolite (BVI; Table 2) shows a drastic change, being strongly depleted in Na_2O and CaO (even by keeping into account the apparent changes related to the strong LOI increase) and enriched in Fe_2O_3 (Fig. 3a, b).

The transition to the overlying lateritic profile involves the drastic disappearance of CaO, Na_2O and MgO; conversely some K_2O, though strongly depleted, can still be detected in the deepest part of the profile (i.e. in the lower kaolinite horizon; Fig. 3c). Figs. 3 and 4 clearly show that the more important variations in the chemical composition along the profile are first of all evidenced by an increase in the Fe_2O_3 content coupled with a decrease in Al_2O_3. This trend becomes significant starting from the base of the mottled horizon upwards. In the uppermost duricrust (BIa), the Fe_2O_3 content is almost 55%, whereas SiO_2 falls down to less than 20% (Table 2; Fig. 3a). Al_2O_3 and TiO_2 show similar patterns (Fig. 3b): their amounts moderately increase moving from the bedrock to the lower part of mottled horizon, whereas they decrease in the upper horizons until values similar to those of the bedrock are reached. According to the Schellmann (1983, 1986) classification, most samples of the Balkouin lateritic profile belong to the category of weak lateritization; only the uppermost horizons (Fe-rich duricrust and upper mottled horizon), conversely, fall into the fields of moderate to strong (BIa) lateritization (Fig. 4).

FIG_4

4.1.2. Trace and Rare Earth elements

Among the trace elements, Rb, Sr and Ba display a concentration pattern similar to those of the major soluble elements such as Ca, Na, Mg and K, as their concentrations strongly decrease from the bedrock upwards (Fig. 3d). Zr, Nb and Y behave instead as relatively insoluble elements, showing (with the exception of saprolite, whose composition is discussed below) strongly similar patterns characterized by an abundance peak in the clay-rich horizon (Fig. 3e). Particularly, a relatively high correlation exists between Zr, Ni, Hf, Y, Nb and Ti, in agreement with their immobile behaviour (Fig. 5; see discussion). Th and U display a similar composition profile, their concentration steadily increasing from the bedrock upwards with a concentration peak located in the clay-rich horizon (Fig. 3f); the same elements show conversely an opposite behaviour at the top of the lateritic profile (pisolitic laterite: sample BIa), where a significant Th increase is coupled to a strong U decrease, in agreement with its mobile behaviour (as U^{+6}) in oxidizing surface conditions.

FIG_5

As shown in Fig. 6, all laterite horizons display a strongly similar REE pattern. In particular, the two bedrock samples (BVIIa and BVIIb, Fig. 6b; Table 2) show the lowest REE content and a moderate LREE/HREE enrichment (La_N/Lu_N=18.2-18.4). Their related patterns are virtually the same, the only difference being a slightly more REE-enriched character of BVIIb and a small Eu positive anomaly in BVIIa. As the medium- to fine-grained biotite ± amphibole granodiorite identified by the BVIIa label is the dominant rock-type of the basement, the REE pattern of the laterite samples will be compared with that of this specimen hereinafter.

FIG_6

FIG_7

Apart from the Fe-rich duricrust, all the laterite horizons show moderate REE enrichments. In particular, when normalized with respect to the bedrock (Fig. 7) most laterite horizons exhibit a sort of flattened V-shaped REE profile, characterized by the occurrence of a negative Eu anomaly (Eu/Eu*= 0.67-0.81) and the enrichment of both the heavier and lighter REE's (La_N/Eu_N=1.37-3.53, Eu_N/Lu_N=0.31-0.50). Specimens from the clay-rich horizon (BIVb and, above all, BIVa) show the highest enrichments. The uppermost laterite horizon (BIa) shows instead LREE contents similar to the bedrock and a moderate HREE enrichment. Apart from the saprolite (see below), the strong Ce anomaly often reported for other lateritic profiles (e.g., Braun et al., 1990; Dequincey et al., 2002) is not observed in the laterite samples from the Balkouin area.

The saprolite specimen (BVI) shows peculiar features, being characterized by anomalous Ba, Y, Zn and REE contents (Table 2 and Figs. 6 and 7). The shape of the related chondrite-normalized REE pattern is broadly similar to that of the bedrock: although displaying a strong negative Ce anomaly, such a profile shows in fact an analogous LREE/HREE enrichment (La_N/Lu_N=22.6). In spite of such similarities, however, the saprolite pattern is shifted to almost ten times higher REE values with respect to the bedrock. These features suggest that the saprolite specimen, collected South-East of Balkouin, possibly represents a more differentiated magmatic facies than the bedrock: aplitic bodies are, in fact, quite common within the granite-granodiorite basement (Plate 1l). Alternatively, REE's could have been trapped by smectites (i.e., in nontronites: see below) of this horizon.

4.2. Mineralogical composition of the lateritic profile

The average mineral composition of the laterite horizons, obtained by thoroughly combining XRPD, SEM-EDS and micro-Raman evidences, is summarized in Table 3. According to their mutual quantities, minerals can be divided into major (>10% in volume), minor (1-10%) and accessory (<1%) phases.

TABLE_3

4.2.1. Major and minor mineral components

The quantitative distribution (expressed as wt%) of both the major and minor mineral components, as detected by XRPD, was calculated for the whole sequence through full profile fitting analyses based on least squares procedures (Rietveld method). Such an approach allows an adequate description of the most significant trends of variation existing throughout the investigated profile. Despite its monotony (ubiquitous presence of four minerals: hematite, goethite, kaolinite and quartz), the mineralogical composition of the laterite evidences peculiar fluctuations of these phases mutual quantities. The results obtained for each specimen are reported in Table 4. The detected trends of variations in the mineralogical composition, expressed as weight % as inferred by XRPD, are summarized in Fig. 8a. In Fig. 8b the comparison between the experimentally observed diffraction patterns with those computed by means of the Rietveld method is shown for selected samples (BVI; BVa; BIIc; BIa). Accuracy for the obtained mineralogical estimates is certified by the excellent fit between experimental and calculated data, the related difference curves (below each pattern) being almost straight. In order to facilitate reading, in each diffraction pattern the main reflections are assigned to the corresponding mineral phase [abbreviations taken from Whitney and Evans (2010), except for Nontronite (Nntr)].
Proceeding from bottom to top, the following aspects can be emphasized:
TABLE_4

- XRPD confirms the granodioritic nature of the *bedrock*, as both analyzed specimens (BVIIa and BVIIb) are rich in albitic plagioclase and quartz, with subordinate K-feldspar (Table 4).

- The composition of saprolite (sample BVI: albitic plagioclase, quartz and nontronite; Table 4) inevitably (though not exclusively) depends on the nature of the underlying bedrock and significantly differs from the above lateritic levels. As hinted above, the strongly enriched REE pattern of BVI suggests that such a specimen represents a more differentiated magmatic facies than the bedrock.

Presence of nontronite (typical formula $Na_x{}^{VI}(Fe,Al,Mg)_2{}^{IV}(Si,Al)_4O_{10}(OH)_2 \bullet nH_2O$ – ^{VI} and ^{IV} representing octahedral and tetrahedral sites respectively and x varying from 0.1 to 0.3: Whittington et al., 2003; Keeling et al., 2000; Scarlett et al., 2008) is not unusual, as such a clay mineral (a Fe-rich term of the smectite group) is commonly present in laterites of Western Australia exploited as nickel ores (McDonald and Whittington, 2008; Gaudin et al., 2005). Its detection, however, is not trivial as it causes severe problems in mineralogical quantitative analyses (Elliot et al., 2009; Scarlett et al., 2008). Nontronite is considered as a phase with 'partial or no known crystal structure' (PONKCS); due to swelling, its chemistry can be altered consequent to cations substitution and assorted hydration states. This implies a significant increase in the c_0 cell parameter (caused by hydration of the interlayer cations) with consequent variation of the (001) basal reflection in the range 9.7-15 Å (Ufer et al., 2008; Bayliss, 1989; Besson et al., 1983; Eggleton, 1977; Keeling et al., 2000; Tsipursky and Drits, 1984; Dekov et al., 2007) or even more (Scarlett et al., 2011). Furthermore, the XRPD signature of nontronite presents asymmetric peak shapes and anisotropic peak broadening (see Figure 8b; sample BVI – reflection labeled 'Nntr') due to turbostratic disorder, namely a random rotation/translation of the individual layers relative to each other (Warren, 1941; Biscoe and Warren, 1942). A preliminary attempt to fit the reflections of the investigated nontronite with the dehydrated model proposed by Manceau et al. (1998) proved to be inadequate, due to strong disagreement in the c_0 values (9.78 vs 14.78 Å respectively). An alternative procedure was therefore needed. Recently the content of nontronite in a lateritic ore from the Bulong mine (Western Australia) was quantified by using two modified models for the PONKCS method, including two Pawley phase lattice models and a peaks phase group model (Wang et al., 2011). In the studied saprolite, however, the observed peak asymmetry due to turbostratic disorder and c_0 discrepancy for nontronite was successfully fitted by adopting the supercell approach suggested by Ufer et al. (2004), applicable to any Rietveld-performing software package. Such a procedure allowed to properly quantify the nontronite content in saprolite (12 wt%)

as well as the residual components (albitic plagioclase ≅ 41 wt%; quartz ≅ 46 wt%). No kaolinite was detected (Table 4; Fig. 8b, sample BVI).

Proceeding upwards in the lateritic sequence horizons, a strong mineralogical change is observed. The most significant aspects can be thus summarized:

FIG_8

1. *Kaolinite horizon*: divided in two layers. In the deeper one no red nor yellow ochres appear – a feature exclusive of the very bottom of the lateritic sequence (specimen BVb). Quartz and a significant clay fraction formed by sole kaolinite prevail, the former being slightly higher (55 vs 44 wt%). Traces of rutile (< 1wt%) are also observed, as confirmed by SEM-EDS and micro-Raman. In the upper layer (sample BVa) the typical mineralogical composition of laterite appears, basically maintained throughout all the upper horizons despite more or less pronounced quantitative variations. Both goethite and hematite are present, the former more abundant (13 vs. 6 wt%; Table 4). Presence of about 20 wt% of red/yellow ochres causes quartz and kaolinite to proportionally decrease with respect to the deeper layer.
2. *Clay-rich horizon*: both investigated specimens (BIVb and BIVa) show red/yellow ochres amounts rather consistent with the underlying kaolinite horizon (almost 20 wt%, with roughly equivalent fractions). The kaolinite content tends be higher in the lower BIVb portion (≅ 62 wt%) at quartz own expense (≅ 18 wt%). The upper part of the horizon (BIVa) shows pronounced analogies with the underlying BVa specimen of the Kaolinite horizon (see Table 4 and Fig. 8a).
3. *Mottled horizon*: in the BIIIb level a drastic decrease in the red/yellow ochres content is observed (< 6 wt%, with goethite prevailing on hematite), as confirmed by its pale colour compared to the reddish hue of the underlying BIVa layer. Transition to the upper BIIIa layer, however, shows a reversed trend which will be maintained for the rest of the sequence, marked by a progressive increase in the red/yellow ochres content (reaching almost 30 wt% in the more superficial BIIc – BIIa levels: Table 4; Fig.8a).
   Transition from the upper 'clay-rich–' (BIVa) to the lower 'mottled horizon' (BIIIb) causes a moderate but progressive raise in the amount of kaolinite (oscillating in the 50-70 wt% range). The amount of quartz, though basically invariant at first (≅ 43 wt% in BIIIb), tends to lower in the upper BIIIa level (≅ 13%) then stabilizing on an average ≅ 20 wt% at the top of the horizon (BIIc – BIIa).
4. *Fe-rich duricrust*: the superficial pisolitic laterite layers (BIb and BIa) show predominance of both red and yellow ochres, whose mutual amounts differ at different depths. In the deeper level (BIb) approximately 20 wt% of both red and yellow ochres coexist, with kaolinite showing no significant variation with respect to the underlying BIIa horizon. The top layer (BIa) shows a heavy red hue due to abundant hematite (> 50 wt%) and subordinate goethite (< 5 wt%) (Fig. 8b; sample BIa, reflections labeled 'Hem' and 'Gth' respectively). A significant kaolinite content (≅ 44 wt%) is preserved, but quartz becomes negligible (< 2%).

Further information about the particular distribution of major and minor minerals along the lateritic profile is also provided by micro-Raman and SEM-EDS evidences. The former technique, for example, can easily discriminate red from yellow ochre – whose microanalytical recognition is not always easy, particularly in fine-grained intergrowths – as the related Raman signatures are clearly identifiable (Figs. 9a and 9b). Moreover, micro-Raman spectroscopy is an efficient tool for unambiguously detect presence of kaolinite in particular sites, as occurrence of such a clay mineral is justified by a doublet in the second-order region (around 3620-3690 cm^{-1}: Frost, 1995; Frost and Van der Gaast, 1997), weak but visible even in complex samples (Fig. 9c).

SEM-EDS observations emphasized the very fine-grained texture of the studied rocks: the chemical composition of spot analyses (beam diameter: few μm), in fact, can often be retraced to a

mixture of different phases. Despite possible contaminations by surrounding grains, however, the correlations between different elements can lead to a feasible recognition of the main minerals identified through XRPD and Raman.

4.2.2. Accessory mineral components

Selected micro-Raman and SEM-EDS evidences, besides confirming the occurrence and distribution of major and minor mineral components, particularly helped in detecting those accessory minerals possibly neglected by XRPD.

Micro-Raman analyses of tiny intergrowths allowed the unambiguous identification of TiO_2 polymorphs along the profile, such as rutile (mottled and kaolinite horizons, hinted by XRPD) and anatase (clay-rich and kaolinite horizons). The latter phase was detected in small grains and identified by the appearance of strong peaks at around 150, 400, 520 and 640 cm^{-1} (Fig. 9d). Besides, micro-Raman was extremely useful in order to exclude presence, in quantities below the XRPD detection threshold, of gibbsite or other Al-rich oxide phases like bohemite and diaspore – typical components (especially the first) of laterites.

FIG_9

SEM-EDS spot micro-analyses allowed sharp identification of further accessory minerals undetected by XRPD, such as:

- apatite, whose presence is suggested by the simultaneous increase of both CaO and P_2O_5 amounts, often detected in samples from the Fe-rich duricrust and mottled horizons. It probably represents a relict phase;
- zircon, a typical relict mineral of laterites, unequivocally identified in the kaolinite horizon;

- a Cu-Sn phase occurring as very small grains (≤ 1-2 μm), locally appearing in the mottled and clay-rich horizons, strongly enriched in Cu (34.5-59.8 wt%) and Sn (7.6-11.6 wt%) together with variable amounts of Fe (7.1-14.3 wt%), Si (1.6-3.0 wt%), Al (2.3-3.5 wt%) and O (12-13 wt%; energy spectrum shown in Fig. 10). Straight identification of such a phase is troublesome as the small size of these grains causes the spot analyses to be contaminated by the host matrix, composed of kaolinite and Fe oxide/hydroxide. Moreover, chemical analyses were performed on the rough surface of broken rock chips and therefore have to be considered only semi-quantitative. Attempts to acquire Raman spectra were so far unsuccessful. It is interesting to note, however, that the measured oxygen quantity is very low (i.e. probably related to the matrix) and the Cu/Sn ratio broadly constant (7.9/9.6). These data suggest that this mineral could be a Cu-Sn intermetallic phase, possibly Sn-bearing native copper. Although native copper can occur as a secondary phase in lateritic soils (related to leaching of Cu-bearing sulphides under oxidizing conditions and Cu reprecipitation at shallow depth: Monti, 1987), presence of Sn-bearing native copper was seldom reported in nature (Xie et al., 2006, with refs. therein) but never in laterite. These circumscribed Cu-Sn enrichments could therefore be related to the weathering of low-grade hydrothermal polymetallic mineralizations, possibly occurring in the basement rocks (Castaing et al., 2003a).

FIG_10

SEM-EDS analyses further confirmed presence of possible TiO_2 polymorphs, typical in laterite and identified also by XRPD (i.e. rutile in BVb) and micro-Raman (i.e. anatase in BVa). TiO_2-rich, very fine-grained intergrowths were found in all laterite horizons, clearly as a result of the transformation of primary rutile and/or titanite.

5. Discussion

In the Balkouin area, a basement of granodioritic composition which passes upwards to saprolite is covered by a 10-11 m thick cover of lateritic rocks. Such a cover shows a strong chemical and mineralogical zoning typical of laterite, being almost completely depleted in the soluble elements (K, Mg, Ca, Na, Rb, Sr, Ba), strongly enriched in Fe (in the form of Fe oxide and hydroxide minerals, such as hematite and/or goethite) and progressively impoverished in Si (in the form of quartz) proceeding from bottom to top. Iron (and related oxide/hydroxide), in particular, becomes very abundant in the uppermost profile in which Si has been mostly removed, whereas the Al content (ascribable to a significant clay fraction in the form of kaolinite) does not evidence significant variations throughout all the succession.

Some chemical and mineralogical features (e.g., the strong Fe_2O_3/Al_2O_3 enrichments and consequent abundance of Fe ± Al oxides phases, coupled with a marked SiO_2 decrease proceeding towards the surface) are a common feature of the lateritic profiles worldwide even if, in detail, each profile is unique. As already mentioned, several authors (e.g., Bourman, 1993; Bourman and Ollier, 2002, 2003, with refs. therein) strongly criticized the classic laterite concept largely based on Schellmann studies (and minor later modifications: Aleva, 1994), who kept into account the chemical composition of the weathered rocks in comparison to that of the underlying source rocks. These authors argue, *inter alia*, that many (possibly most) "regolith materials" may form by *lateral* transport, both physical and chemical, rather than chemical evolution along *vertical* directions. In particular, the "so-called laterites" would mainly form as a consequence of the remarkable iron concentration coming from *aside*. The same authors state that only a limited subset of "laterites" may effectively derive from the underlying rock, thus confining the chemical classification conceived by Schellmann to be fit to describe only this restricted group. Such a classification, however, would be impractical in the field and a morphological approach (like the one proposed by Pullan, 1967) should be preferred.

5.1. Protolith of the Balkouin laterite

In the case of the Balkouin laterite, the availability of compositional data from the whole profile (not only on those horizons used as a building material) allows the unequivocal identification of the underlying granodioritic basement as the parent rock. It is well known that the elements properties play a key role in the lateritization process: in particular alkalis and alkaline earths enjoy a strong mobility during lateritization, because they do not form stable secondary minerals. Due to this, they are usually lost from the profile (Fig. 3, Table 2). On the contrary, the HFSEs (particularly Ni, Y, Nb, La, Th, Zr, Ti: Zarasvandi et al., 2010) are generally considered immobile elements during weathering. Binary graphics of major and trace elements plotted against Ti (a highly immobile element) show therefore highly different distribution patterns (Fig. 5), which depend on the element behaviour. As emphasized by several authors (e.g., MacLean et al., 1997; Zarasvandi et al., 2010, 2012), the ratio of immobile elements in the lateritization/bauxitization processes (such as Ti and Zr) will be the same both in the laterite and in the precursor rock. If data on several samples from a laterite profile are available, the ratios of immobile elements should produce highly correlated linear arrays, passing through the origin of the plot. Fig. 5 shows that such a condition is fulfilled for the Balkouin laterite. Basing on these premises, the bedrock can therefore be considered, with all due probability, as the precursor rock of the lateritic sequence as the corresponding data (open squares in Fig. 5) are strictly close to the array in almost all diagrams. The same type of relationship with TiO_2 is broadly followed by other elements such as Ni, Hf, Y, Nb. The partial scattering shown by some of the data in Fig. 5 may be explained by the existence of primary heterogeneities affecting the bedrock composition, an occurrence observed in the field (the bedrock ranges from biotite ± amphibole granite/granodiorite to foliated granodiorite and is crosscut by aplite and/or pegmatite dykes). SiO_2, Al_2O_3 and Fe_2O_3, conversely, show more complicated relationships, as a consequence of a more mobile behaviour (Fig. 5).

A strong additional evidence supporting the hypothesis of the bedrock being the precursor rock of laterite is given by the REE patterns measured for all horizons, which closely match that of the underlying basement (Fig. 6). In fact, the shape of the chondrite-normalized REE patterns of all lateritic horizons is virtually the same, thus implying a direct origin of the sequence from the underlying bedrock. As already discussed, also the protolith of the saprolite sample (BVI), which shows a strong REE enrichment, is probably an intrusive rock pertaining to the same magmatic suite of the host granodiorite, though more differentiated.

5.2. Mass change during lateritization

The unambiguous recognition of the bedrock as the parent rock allows the calculation of the mass change all along the profile, in order to better reconstruct the geochemical processes involved in the development of the Balkouin laterite. The mass change calculation was performed by adopting the immobile element method (MacLean and Kranidiotis, 1987; MacLean, 1990; MacLean et al., 1997), often applied to the problem of bauxite (and, in part, laterite) formation (e.g., MacLean et al., 1997; Liaghat et al., 2003; Zarasvandi et al., 2010, 2012; Liu et al., 2013). Mass changes in mobile elements compared to the protolith (sample BVIIa) were calculated against TiO_2 (considered immobile) from the following relations (MacLean, 1990; MacLean et al., 1997):

EF (enrichment factor) = TiO_2 precursor rock / TiO_2 altered rock

RC (reconstructed composition) = % component in altered rock x EF

MC (mass change) = RC – precursor composition.

The results of the mass change calculation of lateritic horizons with respect to the underlying bedrock are given in Table 5 and displayed (in terms of relative depletion or enrichment of element concentrations) in Fig. 11. Although sample BVIIa is the most reliable candidate as the protolith, variations of element concentrations are shown for both samples BVIIa (dark bars) and BVIIb (light bars). A comparison of the two situations shows that although some differences arise because of the different TiO_2 content, the general trend does not change. By keeping into account the slight heterogeneity existing in the bedrock composition, the effective mass change value must therefore be comprised within those computed for each of the two basement samples (BVIIa and BVIIb). These data emphasize the extent of the mass loss, which exceeds 50 wt% (and often 70 wt%) for almost all horizons, and show that most elements have a similar, coherent depletion trend. Such a behaviour involves not only K, Na, Mg, Ca, P and Mn but also silica and alumina, which evidence an increasing depletion along the medium to upper part of the profile suggesting existence of a near-neutral to acidic oxidizing environment (see below). Conversely, only Fe shows an enrichment which becomes particularly evident in the uppermost horizons. The order of magnitude of the mass change values is consistent with the results of similar calculations performed by other authors on lateritic or (more often) bauxitic rocks (e.g., MacLean et al., 1997; Liaghat et al., 2003; Du et al., 2010; Zarasvandi et al., 2012, 2012; Entezari, 2012; Liu et al., 2013), the latters being of course characterized by a strong Al_2O_3 gain (coupled with a decrease of Fe_2O_3).

TABLE_5

FIG_11

5.3. The laterite forming process

The compositional trends shown in the composition vs. depth plot of Fig. 3 and in the ternary diagram of Fig. 4, in addition to the mass change calculations, provide some additional constraints to the profile development of the Balkouin laterite. As summarized by Eggleton and Taylor (1999), the mechanism according to which a lateritic profile can develop is far from being unanimously accepted, even when assuming that the underlying basement is the parent rock. As stated above, the strong iron loading in the upper part of the profile has been related to residual or absolute vertical enrichment processes (from the underlying layers or from above: Trendall, 1962) as well as possible

lateral sources responsible for the formation of iron- (and aluminium-) rich crusts (e.g. Ollier and Galloway, 1990; Bourman and Ollier, 2002, with refs. therein). The chemical composition pattern of the Balkouin profile (Fig. 3) stresses the intensity of the intervened mobilization processes responsible for the laterite formation. These processes are fully compatible with a progressive compositional change which proceeds from the bottom to the top, due to progressive and selective mobilization and residual concentration processes.

As evident from Table 2 and Figs. 3 and 4, in the transition from granodiorite to saprolite significant compositional variations already occur, which involve an increase in Fe_2O_3 and a strong decrease in Na_2O and CaO contents. Elements other than Al, Si and Fe almost completely disappear from the base of the lateritic profile towards the top. In the lower kaolinite horizon (sample BVb) a significant increase of Al_2O_3 occurs with respect to the underlying bedrock, guaranteed by presence of a conspicuous kaolinite fraction (almost 44 wt%), but the Fe_2O_3 content remains approximately the same – as justified by the lack of appreciable amounts of hematite and/or goethite (Table 4). The chemical trend changes abruptly starting from the upper kaolinite horizon (BVa) upwards: in the Al_2O_3-SiO_2-Fe_2O_3 diagram (Fig. 4) all the overlying horizons are in fact aligned along a narrow band, which broadly maintains a fixed Al_2O_3/SiO_2 ratio and progressively moves towards the Fe_2O_3 apex. Such a trend is confirmed by the detection and progressive enrichment of Fe oxide/hydroxide phases (Table 4 and Fig. 8a). It is interesting to note that such a band roughly coincides with the Al_2O_3/SiO_2 ratio typical of kaolinite (dashed "kaolinite line" in Fig. 4). This compositional trend is in good agreement with an *in situ* lateritization process, in which a lateritic profile develops with progressively increasing weathering (and associated selective leaching) upwards. In such a process a strong decrease in SiO_2 is expected, until kaolinite forms as a stable phase as the result of an Al_2O_3/SiO_2 ratio typical of this clay mineral. Once the Al_2O_3/SiO_2 ratio reaches the interval typical of kaolinite formation, the related value tends to remain broadly constant.

In the underlying saprolite, kaolinite is absent or occurs only as a very minor phase (well below the XRPD detection threshold): the major Al_2O_3 content, in fact, is fixed mainly in an almost exclusively albitic plagioclase and subordinately in nontronite (Table 4). The transition to the overlying lateritic profile marks the breakdown of these phases, thus allowing kaolinite to become one of the major components upwards.

A detailed observation of the diagram in Fig. 4 shows that in the Balkouin profile the Al_2O_3/SiO_2 ratio is indeed a bit lower than that typical of kaolinite – those symbols ascribed to the analyzed samples being actually slightly above the dashed "kaolinite line". Such an occurrence is due to the fact that, as shown by XRPD, part of the silica occurs in the form of residual quartz (and possibly amorphous silica too). Once the proper ratio for the crystallization of kaolinite is reached, the subsequent transformations mainly involve its progressive dissolution with an increase in Fe_2O_3 content upwards while maintaining a generally constant SiO_2/Al_2O_3 ratio – with the exception of the Fe-rich duricrust, where silica is strongly leached (i.e. Fig. 3a). Kaolinite dissolution processes (both congruent and incongruent), based also on experimental studies, were suggested by several authors (Gardner, 1970; Carroll and Walther, 1990). As already emphasized, all performed analyses point to the absence in the profile of Al-bearing oxide phases (like, for example, gibbsite, bohemite and diaspore). Lack of these phases is consistent with the thermodynamic mechanisms proposed in literature, according to which gibbsite cannot form consequent to dissolution of kaolinite unless quartz is absent (and other specific conditions are encountered: Gardner, 1970). This is consistent with the collected XRPD data, which unequivocally show presence of excess silica (in the form of quartz) all along the lateritic profile.

The prospected hypothesis of laterite formation as the result of *in situ* residual enrichment processes is consistent with the collected trace elements geochemistry data. Within every lateritic profile, in fact, strong variations in the Eh-pH conditions occur which can strongly influence the elements mobility. Among the REE, which generally show a strongly coherent behaviour in natural systems, cerium is particularly affected by the Eh variations because it can occur both as Ce^{3+} (like most of lanthanides) and – in oxidizing conditions – as Ce^{4+} (Braun et al., 1990). As a consequence,

any process during laterite formation involving external sources (as solutions and/or solids: Bourman and Ollier, 2002) would probably generate a strong anomaly (positive or negative) in cerium, due to its peculiar behaviour. Such a strong Ce anomaly however, which is a distinctive feature of some laterites (Braun et al., 1990; Dequincey et al., 2002), does not occur in the horizons from the Balkouin lateritic profile, implying that no external influence possibly affected its genesis.

As hinted above, however, the prospected phenomena which possibly justify the formation of the Balkouin laterite (continuous, *in situ* residual enrichments free from external sources) cannot be thoroughly transposed onto other latériric sequences – not even in this specific geographic area. A detailed study (based also on isotopic data) performed at Kaya, north-eastern Burkina Faso, by Dequincey et al. (2002) on a laterite developed – like the one from Balkouin – on a Birimian granodiorite basement, led in fact to hypothesize a different and complex formation history. For this lateritic profile, composed of different petrological units, a discontinuous genesis, developed under different weathering conditions, was suggested due to mineralogical evidences such as occurrence of weatherable minerals (i.e. kyanite, staurolite and hornblende) in the iron cap. Alternative processes to explain laterite genesis were also hinted by other studies in Western and Central Africa. Nguetnkam et al. (2006), for instance, call into question a polyphasic process to explain formation of a lateritic profile in Cameroun, as emphasized by strong geochemical discontinuities within the profile evident in the Al_2O_3-SiO_2-Fe_2O_3 diagram. In other studies multistage processes were suggested by the occurrence of stratigraphic anomalies within the lateritic profile (e.g., Sastri and Sastry, 1982).

Apparently none of these processes seem to apply to the Balkouin profile, for which no strong petrological, geochemical or stratigraphic inconsistency was found. Besides, a laterite like that described by Dequincey et al. (2002), which actually crops out at higher altitude, could represent an older sequence which experienced a more complex weathering evolution. It is well known, in fact, that several types of lateritic rocks, with different characters and age (from Upper Cretaceous to Quaternary) occur in West Africa – including Burkina Faso (Marcelin, 1971; Hottin and Ouedraogo, 1975; Sattran and Wenmenga, 2002). Alternatively, the relics of a prolonged evolution may have been partially obliterated by the mobilization/remobilization processes connected with lateritization (e.g., Beauvais, 1999; Dequincey et al., 2002).

5.4. The laterite-forming environment

The genesis and the characters of laterite (as well as bauxite) depend on several variables, including climate, characters of the bedrock and groundwater quality (Norton, 1973). In the Balkouin area the current climatic conditions (actual average annual temperature and rainfall, respectively, of ca. 28.8°C and 900 mm) match those suggested by Tardy (1993: ca. 28°C, low humidity) as typical laterite-forming conditions, opposed to those (ca. 22°C and high humidity) attending the formation of bauxite. The groundwater quality is of paramount importance: in fact, selective removal from the soil of alkalis, alkali earths and silicon with consequent enrichment in Fe and/or Al is accomplished by having a precise combination of Eh and pH.

The approximate conditions for the formation of the Balkouin laterite can be inferred from the analysis of the Eh-pH diagram of Fig. 12a (from Norton, 1973), where the solubility contours for Fe and Al (in moles/l) are shown. The diagram is divided into two areas by a curve of equal solubility for Al and Fe oxides and hydroxides ($\Sigma Al = \Sigma Fe$). At low Eh and pH values (darker area) Fe minerals are more soluble, whereas above this line (lighter area) gibbsite is more soluble. On the right of the dotted line the solubility of both Fe and Al is very low, thus suggesting that laterite (or bauxite) will result only if the protolith is relatively rich in Fe (or Al). The location of the pH-dependent kaolinite-in and kaolinite-gibbsite curves is also shown: their locations are highly approximate, being a function of the fluid composition (Dangic, 1985). The conditions of formations of the Balkouin laterite must lie outside the isosolubility curve, where Al minerals are more soluble than Fe minerals; considering that the bedrock protolith has a very low Fe/Al ratio

(Fe_2O_3/Al_2O_3 = 0.12), the laterite formation must have occurred at low pH (≤4.5) and high Eh (≥ 0.4) values, i.e., under acidic and oxidizing and conditions (dark grey area in Fig. 12b). The breakdown of kaolinite in the uppermost laterite horizons without appearance of gibbsite may have been favoured by pH decrease; alternatively, the high concentration of dissolved SiO_2 may have been inhibited by precipitation of gibbsite, favouring instead the removal of Si and Al at similar rates (Meillon, 1978). These inferred conditions obviously differ from those calculated by other authors for the formation of bauxite (light grey area in Fig. 12b: Temur and Kansun, 2006; Zarasvandi, 2012; Liu et al., 2012, 2013), which instead requires selective leaching of Fe (apart from Si) generally obtained under more reducing conditions and higher pH.

FIG_12

6. Conclusions

A lateritic profile resting above a granodioritic basement and cropping out in the Balkouin area, Central Burkina Faso, was studied with a multidisciplinary analytical approach in order to infer the processes responsible for its genesis and the possible constraints to its development.

From bottom to top, the investigated profile shows a strong chemical and mineralogical zoning. The saprolite, mainly composed of quartz, albite and subordinate nontronite, shows significant variations with respect to the underlying bedrock, with strong depletion in Na, Ca and Sr and enrichment in Fe. The transition to the overlying lateritic horizons implies the establishment of an almost constant mineral assemblage (quartz, kaolinite, goethite and hematite) marked by a quantitative variational trend which involves a progressive quartz decrease coupled to an increase in goethite/hematite. In the deepest part of the lateritic profile Ca, Na and Mg almost disappear, whereas some K and Ba, though depleted, still occur. Mass change calculations indicate a strong depletion of the major elements from the profile, with strong losses of Si, Al, Ca, Na, K and Mg while proceeding upwards. Only Fe shows a drastic enrichment, particularly at top of the profile, consistently with the predominance of goethite and (especially) hematite.

Analyses of trace and RE elements strongly suggest an autochthonous origin for the investigated laterite. In fact, binary plots of immobile elements such as Zr, Ni, Hf, Y, Nb against Ti evidence highly correlated linear arrays. Moreover, the pattern of the REE – which show moderate enrichments in the lateritic layers - closely matches that of the underlying bedrock.

Mineralogical and geochemical data suggest that lateritization developed as a continuous process, with weathering and associated selective leaching gradually increasing upwards and finally leading to the strong Fe enrichment and Si depletion observed in the superficial Fe-rich duricrust. The development of the Balkouin laterite is therefore compatible with the classic Schellmann genetic model, although such a process does not rule out the possible existence of different mechanisms operating in other situations, particularly for “allochthonous” laterite.

In the Balkouin lateritic profile gibbsite and bohemite do not occur. Even in the most enriched sequences (clay-rich and mottled horizons), in fact, all Al appears as kaolinite and the global Al_2O_3 content remains relatively low, possibly as a consequence of some Al removal too (as hinted by mass change calculations). The observed analogies between the Al_2O_3 and the SiO_2 profiles – particularly for those levels positioned above the clay-rich horizon – suggest concomitant removal of both Al and Si possibly related to kaolinite dissolution, in the upper part, with all due probability related to a process of colloidal mobilization like that described by Malengreau and Sposito (1997). A further parameter possibly inhibiting the formation of free aluminum hydroxides is represented by the silica-rich composition of the bedrock (granodiorite), which causes quartz (and possibly also amorphous silica) to be generally present, though progressively depleted, all along the profile.

At Balkouin the lateritization process occurred despite the very low Fe/Al ratio and caused formation of strong Fe enrichments in the upper horizons. This fact strongly emphasizes the

importance of the “groundwater quality” (in terms of Eh and pH) as a main factor controlling – in proper climatic conditions - the geochemical features of the residual soil. The composition of the Balkouin laterite, developed at the expenses of a granodioritic bedrock, requires strongly selective removal of Si and Al coupled with retention of Fe, which can only occur under oxidizing and acidic conditions. The Eh and pH conditions, more than the protolith composition itself, appear therefore as determining factors for the formation of a Fe-rich laterite (or alternatively bauxite, in a different context) like the one studied here.

Acknowledgements

The paper benefited from the constructive comments of Prof. A. Zarasvandi, an anonymous reviewer and of the journal editor, who are gratefully acknowledged. We are most grateful to all the staff of the LEMC (Laboratoire d’Eco-Matériaux de Construction) of the 2iE (Institut International d’Ingénierie de l’eau et de l’Environnement) for the help during the field activities. The micro-Raman measures have been collected with the equipment acquired by the Interdepartmental Center “G. Scansetti” for Studies on Asbestos and Other Toxic Particulates with a grant from Compagnia di San Paolo, Turin, Italy.

Appendix

Whole rock analyses were obtained at ALS Chemex, Sevilla, using ICP-AES and ICP-MS techniques for major and trace elements, respectively. Detection limit for major elements is 0.01 wt% oxide, those for trace elements (collected according to the ME-MS81 Chemex protocol) are detailed in the ALS Chemex web page.

Mineral analyses were obtained using a SEM Cambridge Stereoscan 360 equipped with an EDS Energy 200 and Pentafet Detector (Oxford Intruments) installed at the Department of Earth Sciences, Turin. Operating conditions were 15 kV accelerating potential and 50 s counting time. Natural and synthetic mineral and oxide standards were employed and raw data were corrected using the INCA Suite v. 4.01.

X-ray powder diffraction (XRPD) data were collected on specimens preliminarily crushed using an agate mortar and pestle. Diffractograms were collected in the 3-70° 2θ range at room temperature, using an automated Siemens D-5000 diffractometer with a $\theta/2\theta$ setup in Bragg-Brentano geometry, using graphite monochromatized Cu-Kα radiation and a zero-background flat sample holder. Qualitative mineralogical analyses were obtained using the Diffrac Plus (2005) evaluation package – EVA 11,00,3. Quantitative X-ray diffraction data were obtained by means of model-constrained, full pattern analyses with the Rietveld method using the GSAS software package (Larson and Von Dreele, 2007) equipped with the EXPGUI graphical user interface (Toby, 2001). Crystallographic information files (‘cif’) were taken from Levien et al. (1980; quartz), Bish and Von Dreele, (1989; kaolinite), Blake et al. (1966; hematite), Gualtieri and Venturelli, (1999; goethite), Baur (1956; rutile), Harlow and Brown (1980; albite), Angel (1988; anorthite), Prince et al. (1973; orthoclase), Brigatti et al. (2000; biotite), Oberti et al. (1995; Mg-hornblende).

Micro-Raman spectroscopy was performed with a LabRAM-HR 800 (HORIBA - JOBIN-YVON) spectrometer at the Dept. of Earth Sciences, Turin, using a Nd solid state laser (532 nm, 100 mW).

References

Aleva, G.J.J., 1994. Laterites. Concepts, Geology, Morphology and Chemistry. ISRIC, Wageningen.

Angel, R.J., 1988. High-pressure structure of anorthite. American Mineralogist 73, 1114-1119.

Baur, W.H., 1956. Uber die verfeinerung der kristallstrukturbestimmung einiger vertreter des rutiltyps: TiO_2, SnO_2, GeO_2 und MgF_2. Acta Crystallographica 9, 515-520.

Bayliss, P., 1989. Unit-cell determinations of two-dimensional clay minerals. Powder Diffraction 4, 19-20.

Beauvais, A., 1999. Geochemical balance of lateritization processes and climatic signatures in weathering profiles overlain by ferricrete in Central Africa. Geochimica et Cosmochimica Acta 63, 3939– 3957.

Besson, G., Bookin, A.S., Dainyak, L.G., Rautureau, M., Tsipursky, S.I., Tchoubar, C., Drits V.A., 1983. Use of diffraction and Mössbauer methods for the structural and crystallochemical characterization of nontronites. Journal of Applied Crystallography 16, 374-383.

Biscoe, J., Warren, B.E., 1942. An X-ray study of carbon black. Journal of Applied Physics 13, 364-371.

Bish, D., Von Dreele, R.B., 1989. Rietveld refinement of non-hydrogen atomic positions in kaolinite. Clays and Clay Minerals 37, 289-296.

Blake, R.L., Hessevick, R.E., Zoltai, T., Finger, L.W., 1966. Refinement of the hematite structure. American Mineralogist 51, 123-129.

Bourman, R.P., 1993. Perennial problems in the study of laterite: a review. Australian Journal of Earth Sciences 4, 387– 401.

Bourman, R.P., Ollier, C.D., 2002. A critique of the Schellmann definition and classification of ‘laterite’. Catena 47, 117-131.

Bourman, R.P., Ollier, C.D., 2003. Reply to the discussion of ‘‘A critique of the Schellmann definition and classification of laterite’’ by R.P. Bourman and C.D. Ollier (Catena 47, 117–131). Catena 52, 81-83.

Braun, J.J., Pagel, M., Muller, J.P., Bilong, P., Michard, A., Guillet, B., 1990. Cerium anomalies in lateritic profiles. Geochimica et Cosmochimica Acta 54, 781-795.

Brigatti, M.F., Frigieri, P., Ghezzo, C., Poppi L., 2000. Crystal chemistry of Al-rich biotites coexisting with muscovites in peraluminous granites. American Mineralogist 85, 436-448.

Buchanan, F.H., 1807. A journey from Madras through the Countries of Mysore, Kanara and Malabar, 2nd vol., East India Co, London.

Carroll, S.A., Walther, J.V., 1990. Kaolinite dissolution at 25°, 60°, and 80°C. American Journal of Science 290, 797-810.

Castaing, C., Chevremont, P., Donzeau, M., Egal, E., Le Metour, J., Thieblemont, D., Tegyey, M., Guerrot, C., Billa, M., Itard, Y., Delpont G., Ki, J.-C., Zunino, C., 2003a. Notice Explicative de la Carte Géologique du Burkina Faso à l’échelle 1/200.000, Sheet Ouagadougou, BRGM (Ed.), Orléans.

Castaing, C., Chevremont, P., Donzeau, M., Egal, E., Ouedraogo, I., Kote, S., Kabore, E.B., Billa, M., Zida, B., 2003b. Carte Géologique du Burkina Faso à l’échelle 1/200.000, Sheet Ouagadougou, BRGM (Ed.), Orléans.

Dahanayake, K., 1982. Laterites of Sri Lanka- A Reconnaissance Study. Mineralium Deposita 17, 245-256.

Dangic A., 1985. Kaolinization of bauxite: a study in the Vlasenica bauxite area, Yugoslavia. I. Alteration of the matrix. Clays and Clay Minerals 33, 517-524.

Dekov, V.M., Kamenov, G.D., Stummeyer, J., Thiry, M., Savelli, C., Shanks, W.C., Fortin, D., Kuzmann, E., Vértes, A., 2007. Hydrothermal nontronite formation at Eolo Seamount (Aeolian volcanic arc, Tyrrhenian Sea). Chemical Geology 245, 103-119.

Dequincey, O., Chabaux, F., Clauer, N., Sigmarsson, O., Liewig, N., Leprun, J.-C., 2002. Chemical mobilizations in laterites: Evidence from trace elements and ^{238}U-^{234}U-^{230}Th disequilibria. Geochimica et Cosmochimica Acta 66, 1197–1210.

Diffrac Plus Evaluation Package, 2005. EVA, 11, 0, 0, 3. Copyright © SOCABIM 1996-2005.

Du, X., Rate, A.W., Gee, M., 2010. Geochemical mass-balance in intensely weathered soils, Darling Range, Western Australia. Proc. 19th World Congress of Soil Science, Soil Solutions for a Changing World, Brisbane, Australia, publ. on DVD.

Eggleton, R.A., 1977. Nontronite: Chemistry and X-ray diffraction. Clay Minerals 12, 181-194.

Eggleton, R.A., Taylor, G., 1999. Selected thoughts on laterite, in: Taylor, G., Pain, C.F. (Eds.), New approaches to an old continent. CRC LEME, Perth, pp. 209-226.

Elliot, A., Fletcher, H., Li, J., Watling, H., Robinson, D.J., 2009. 39th Annual Hydrometallurgy Meeting and 48th Annual Conference of Metallurgists, Canadian Institute of Mining, Metallurgy and Petroleum, Montreal, pp. 537-549.

Entezari, A., 2012. A Geochemical Survey of the Mandil-Besar Bauxite-Laterite Depositions (South Eastern of Maragheh). European Journal of Scientific Research 70, 361-372.

Fernández-Caliani, J.C., Cantano, M., 2010. Intensive kaolinization during a lateritic weathering event in South-West Spain. Mineralogical and geochemical inferences from a relict paleosol. Catena 80, 23–33.

Frost, R.L., 1995. Fourier Transform raman spectroscopy of kaolinite, dickite and halloysite. Clays and Clay Minerals 43, 191-195.

Frost, R.L., Van der Gaast, S.J., 1997. Kaolinite hydroxyls – A Raman spectroscopy study. Clay Minerals 32, 471-484.

Gardner, L.R., 1970. A chemical model for the origin of gibbsite from kaolinite. American Mineralogist 55, 1380-1389.

Garrels, R.M., Christ, C. L., 1965. Solutions, minerals, and equilibria. Harper and Row, New York.

Gaudin, A., Decarreau, A., Noack, Y., Grauby, O., 2005. Clay mineralogy of the nickel laterite ore developed from serpentinised peridotites at Murrin Murrin, Western Australia. Australian Journal of Earth Sciences 52, 231-241.

Gidigasu, M.D., 1971. The importance of soil genesis in the engineering classification of Ghana soils. Engineering Geology 5,117–161.

Gidigasu, M.D., 1974. Degree of weathering in the identification of laterite materials for engineering purposes – A review. Engineering Geology 8, 213–266.

Giorgis, I., 2012. Caratterizzazione composizionale e geomeccanica della laterite di Balkouy (Burkina Faso). Unpublished MSc Thesis, University of Turin, 158 p.

Gualtieri, A., Venturelli, P., 1999. In situ study of the goethite-hematite phase transformation by real-time synchrotron powder diffraction. American Mineralogist 84, 895-904.

Harlow, G.E., Brown, G.E., 1980. Low albite: an X-ray and neutron diffraction study. American Mineralogist 65, 986-995.

Hieronymous, B., Kotschoubey, B., Boulègue, J., 2001. Gallium behaviour in some contrasting lateritic profiles from Cameroon and Brazil. Journal of Geochemical Exploration 72, 147-163.

Hottin, G., Ouedraogo, O.F., 1975. Notice explicative de la carte géologique à 1:1000.000 de la République de Haute-Volta. Dir. Géol. et des Mines.

Kasthurba, A.K., Santhanam, M., Mathews, M.S., 2005. Investigation of laterite stones for building purpose from Malabar Region, Kerala State- SW India - Part 1: Field studies and profile characterization. Construction and Building Materials 21, 73-82.

Kasthurba, A.K., Santhanam, M., Mathews, M.S., 2007. Investigation of laterite stone for building purposes from Malabar region, Kerala state, SW India: Part I – Chemical analysis and microstructure studies. Construction and Building Material 22, 2400-2408.

Keeling, J.L., Raven, M.D., Gates, W.P., 2000. Geology and characterization of two hydrothermal nontronites from weathered metamorphic rocks at the Uley graphite mine, South Australia. Clays and Clay Minerals 48, 537-548.

Larson, A.C., Von Dreele, R.B., 2007. GSAS – General Structure Analysis System. Los Alamos National Laboratory Report No. LAUR 86-748.

Lawane, A., Vinai, R., Pantet, A., Thomassin, J.H., 2011. Characterisation of laterite stone as building material in Burkina Faso: state of the art of the on-going research and its perspectives. Proc. 6ème édition Journées Scientifiques du 2iE, Ouagadougou, pp.1-4.

Lecomte-nana, G.L., Lesueur, E., Bonnet, J.P., Lecomte, G., 2009. Characterization of a lateritic geomaterial and its elaboration through a chemical route. Construction and Building Materials 23, 1126–1132.

Levien, L., Prewitt, C.T., Weidner, D.J., 1980. Structure and elastic properties of quartz at pressure, P = 1 atm. American Mineralogist 65, 920-930.

Liaghat, S., Hosseini, M., Zarasvandi, A., 2003. Determination of the origin and mass change geochemistry during bauxitization process at the Hangam deposit, SW Iran. Geochemical Journal 37, 627-637.

Liu, X., Wang, Q., Feng, Y., Li, Z., Cai, S., 2013. Genesis of the Guangou karstic bauxite deposit in western Henan, China. Ore Geology Reviews 55, 162-175.

Liu, X., Wang, Q.F., Zhang, Q.Z., Feng, Y.W., Cai, S.H., 2012. Mineralogical characteristics of the superlarge Quaternary bauxite deposits in Jingxi and Debao counties, western Guangxi, China. Journal of Asian Earth Sciences 52, 53–62.

MacLean, W.H., 1990. Mass change calculations in altered rock series. Mineralium Deposita 25, 44-49.

MacLean, W.H., Kranidiotis, P., 1987. Immobile elements as monitors of mass transfer in hydrothermal alteration; Phelps Dodge massive sulfide deposit, Matagami, Quebec. Economic Geology 82, 951–962.

MacLean, W.H., Bonavia, F.F., Sanna, G., 1997. Argillite debris converted to bauxite during karst weathering: evidence from immobile element geochemistry at the Olmedo Deposit, Sardinia. Mineralium Deposita 32, 607-616.

Malengreau, N., Sposito, G., 1997. Short-time dissolution mechanisms of kaolinite tropical soils. Geochimica et Cosmochimica Acta 61, 4297-4307.

Manceau, A., Chateigner, D., Gates, W.P., 1998. Polarized EXAFS, distance-valence least-squares modeling (DVLS) and quantitative texture analysis approache to the structural refinement of Garfield nontronite. Physics and Chemistry of Minerals 25, 347-365.

Marcelin, J., 1971. Notice explicative de la carte géologique au 1:200.000 Gaoua-Batié. DGM Haute-Volta, 31 p.

McDonald, R.G, Whittington, B.I., 2008. Atmospheric acid leaching of nickel laterites review. Part I. Sulphuric acid technologies. Hydrometallurgy 91, 35-55.

Meillon, J.J., 1978. Economic geology and tropical weathering. Bulletin of the Canadian Institute of Mining and Metallurgy 71, 61-70.

Millogo, Y., Traoré, K., Ouedraogo, R. , Kaboré, K., Blanchart, P., Thomassin, J.H., 2008. Geotechnical, mechanical, chemical and mineralogical characterization of lateritic gravels of Sapouy (Burkina Faso) used in road construction. Construction and Building Materials 22, 70–76.

Monti, R., 1987. The Boddington lateritic gold deposit, Western Australia: a product of supergene enrichment processes, in: Ho, S.E., Groves, D.I. (Eds.), Recent advances in understanding Precambrian gold deposits. University of Western Australia Publication Number 11, Nedlands, pp. 355-368.

Nakamura, N., 1974. Determination of REE, Ba, Fe, Mg, Na, and K in carbonaceous and ordinary

chondrites. Geochimica et Cosmochimica Acta 38, 757–775.

Nguetnkam, J.P., Yongue Fouateu, R., Bitom, D., Bilong, P., Volkoff, B., 2006. Etude pétrologique d'une formation latéritique sur granite en milieu tropical forestier sud-camerounais (Afrique centrale). Mise en évidence de son caractère polyphasé. Etude et Gestion des Sols 13, 89-102.

Norton, S.A., 1973. Laterite and bauxite formation. Economic Geology 68, 353-361.

Oberti, R., Ungaretti, L., Cannillo, E., Hawthorne, F.C., Memmi, I., 1995. Temperature-dependent Al order-disorder in the tetrahedral double chain of C2/m amphiboles. European Journal of Mineralogy 7, 1049-1063.

Ollier, C.D., Galloway, R.W., 1990. The laterite profile, ferricrete and unconformity. Catena 17, 97–109.

Ollier, C.D., Sheth, H.C., 2008. The High Deccan duricrusts of India and their significance for the 'laterite' issue. Journal of Earth System Science 117, 537–551.

Prince, E., Donnay, G., Martin, R.F., 1973. Neutron diffraction refinement of an ordered orthoclase structure. American Mineralogist 58, 500-507.

Pullan, R.A., 1967. A morphological classification of lateritic ironstones and ferruginized rocks in Northern Nigeria. Nigerian Journal of Science 1, 161–174.

Robb, L., 2005. Introduction to ore-forming processes. Blackwell Science Ltd, Oxford.

Sastri, G.G.K., Sastry, C.S., 1982. Chemical characteristics and evolution of the laterite profile in Hazaridadar Bauxite Plateau, Madhya Pradesh, India. Economic Geology 77, 154-161.

Sattran, V., Wenmenga, U., 2002. Geology of Burkina Faso. Czech Geological Survey, Prague.

Scarlett, N.V.Y., Madsen, I.C., Whittington, B.I., 2008. Time-resolved diffraction studies into the pressure acid leaching of nickel laterite ores: a comparison of laboratory and synchrotron X-ray experiments. Journal of Applied Crystallography 41, 572-583.

Scarlett, N.V.Y., Raven, M., Madsen, I., 2011. Powder X-Ray Diffraction Study of the Hydration and Leaching Behavior of Nontronite. Clays and Clay Minerals 59, 560-567.

Schellmann,W., 1983. A new definition of laterite, in: Hauser, G. (Ed.), Natural Resources and Development, Metzingen, 18, 7-21.

Schellmann, W., 1986. A new definition of laterite. Geological Survey of lndia Memoir 120, 1-7.

Schellmann, W., 2003. Discussion of ''A critique of the Schellmann definition and classification of laterite'' by R.P. Bourman and C.D. Ollier (Catena 47, 117–131). Catena 52, 77-79.

Tardy, Y., Boeglin, J.-L., Novikoff, A., Roquin, C., 1993. Petrological and geochemical classification of laterites. Proceedings 10th International Clay Conference, Adelaide, Australia, p. 481-486.

Temur, S., Kansun, G., 2006. Geology and petrography of the Masatdagi diasporic bauxites, Alanya, Antalya, Turkey. Journal of Asian Earth Sciences 27, 512–522.

Théveniaut, H., Freyssinet, P., 1999. Paleomagnetism applied to lateritic profiles to assess saprolite and duricrust formation processes: the example of Mont Baduel profile (French Guiana). Palaeogeography, Palaeoclimatology, Palaeoecology 148, 209–231.

Toby, B.H., 2001. EXPGUI, a graphical user interface for GSAS. Journal of Applied Crystallography 34, 210-213.

Trendall, A.F., 1962. The formation of apparent peneplains by a process of combined lateritisation and surface wash. Zeitschrift für Geomorphologie 6, 183–197.

Tsipursky, S.I., Drits, V.A., 1984. The distribution of octahedral cations in the 2:1 layers of dioctahedral smectites studied by oblique-texture electron diffraction. Clay Minerals 19, 177-193.

Ufer, K., Roth, G., Kleeberg, R., Stanjek, H., Dohrmann, R., Bergmann, J., 2004. Description of X-ray powder pattern of turbostratically disordered layer structures with a rietveld compatible approach. Zeitscrift für Kristallographie 219, 519-527.

Ufer, K., Stanjek, H., Roth, G., Dohrmann, R., Kleeberg, R., Kaufhold, S., 2008. Quantitative phase analysis of bentonites by the Rietveld method. Clays and Clay Minerals 56, 272-282.

Wang, X., Li, J., Hart, R.D., van Riessen, A., McDonald, R., 2011. Quantitative X-ray diffraction phase analysis of poorly ordered nontronite clay in nickel laterites. Journal of Applied Crystallography 44, 902-910.

Warren, B.E., 1941. X-ray diffraction in random layer lattices. Physical Review 59, 693-698.

Whitney, D.L., Evans, B.W., 2010. Abbreviations for names of rock-forming minerals. American Mineralogist 95, 185–187.

Whittington, B., Johnson, J.A., Quan, L.P., McDonald, R.G., Muir, D.M., 2003. Pressure acid leaching of arid-region nickel laterite ore. Part II: effect of ore type. Hydrometallurgy 70, 47-62.

Xie, Y., Hou, Z., Xu, J., Yuan, Z., Bai, G., Li, X., 2006. Discovery of Cu-Zn, Cu-Sn intermetallic minerals and its significance for genesis of the Mianning-Dechang REE Metallogenic Belt, Sichuan Province, China. Science China Earth Sciences 49, 597-603.

Zarasvandi, A., Zamanian, H., Hejazi, E., 2010. Immobile elements and mass changes geochemistry at Sar-Faryab bauxite deposit, Zagros Mountains, Iran. Journal of Geochemical Exploration 107, 77-85.

Zarasvandi, A., Carranza, E.J.M., Ellahi, S.S., 2012. Geological, geochemical, and mineralogical characteristics of the Mandan and Deh-now bauxite deposits, Zagros Fold Belt, Iran. Ore Geology Reviews 48, 125-138.

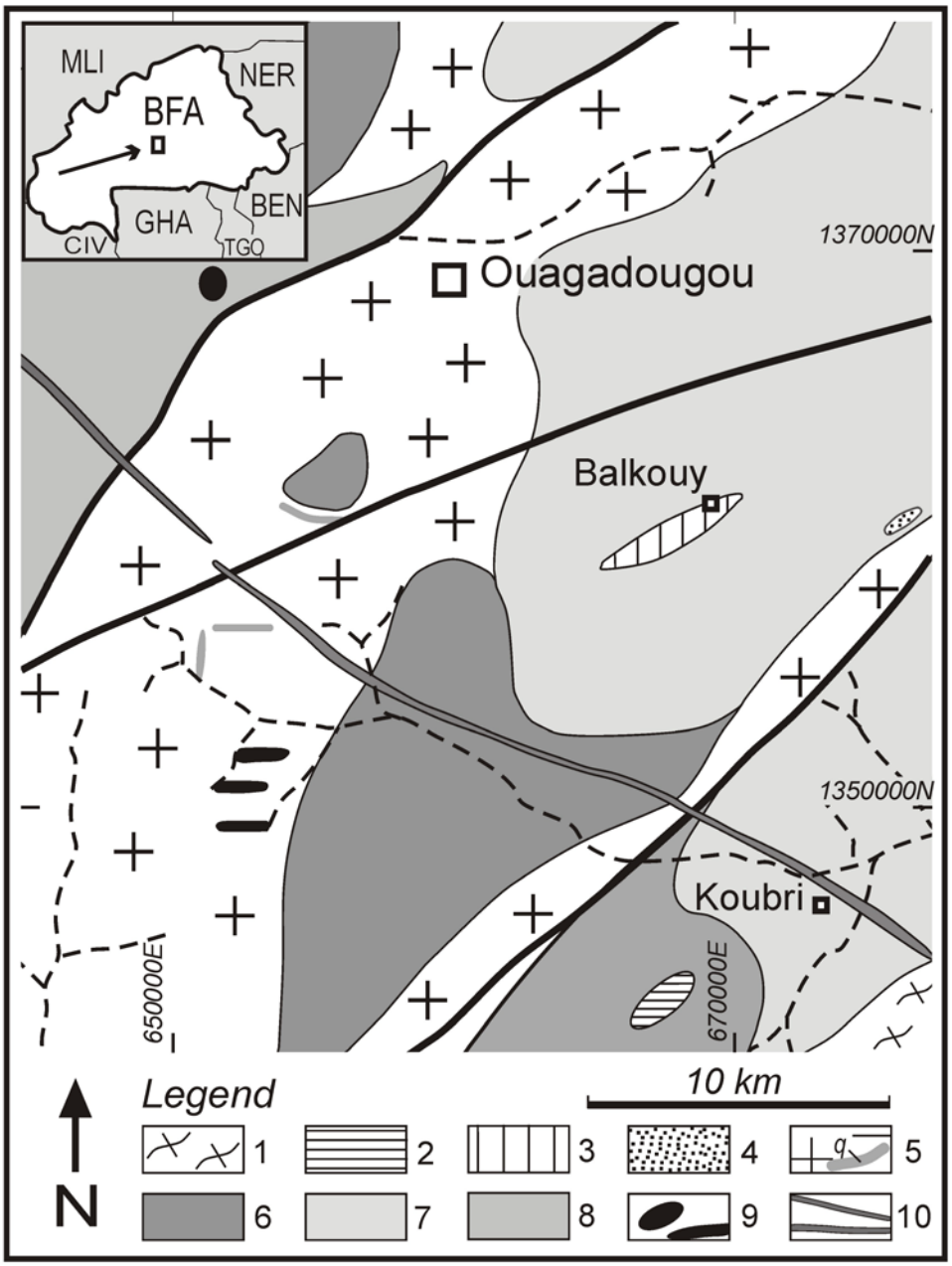
MLI
NER
BFA
BEN
GHA
CIV
TGO
Ouagadougou
1370000N
Balkouy
1350000N
Koubri
650000E
670000E
Legend
10 km
N
1
2
3
4
5
6
7
8
9
10

Fig. 1

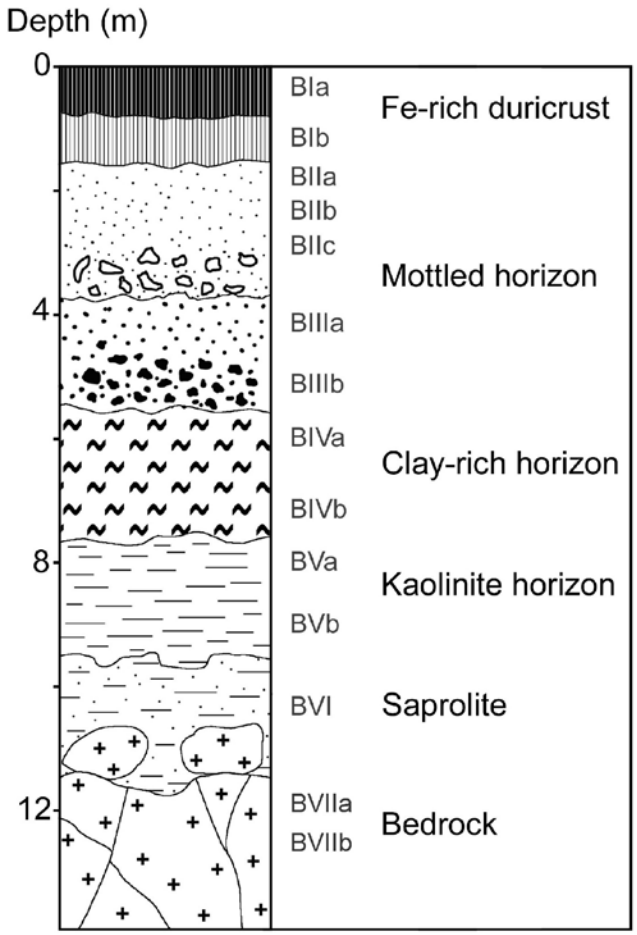
Depth (m)
0
4
8
12
BIa
BIb
BIIa
BIIb
BIIc
BIIIa
BIIIb
BIVa
BIVb
BVa
BVb
BVI
BVIIa
BVIIb
Fe-rich duricrust
Mottled horizon
Clay-rich horizon
Kaolinite horizon
Saprolite
Bedrock

Fig. 2

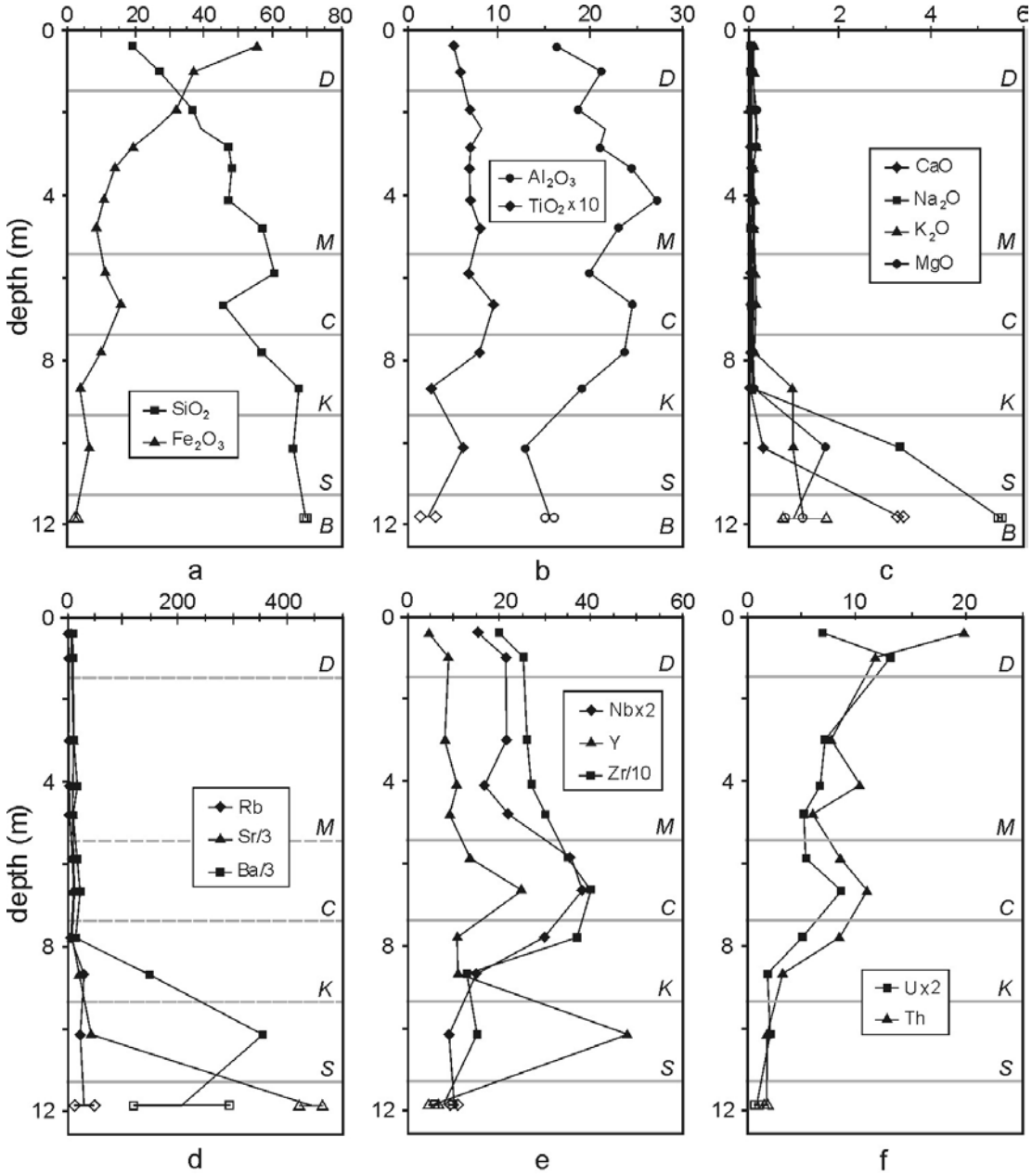
depth (m)
D
M
C
K
S
B
SiO2
Fe2O3
a
Al2O3
TiO2 x 10
b
CaO
Na2O
K2O
MgO
c
Rb
Sr/3
Ba/3
d
Nbx2
Y
Zr/10
e
Ux2
Th
f

Fig. 3

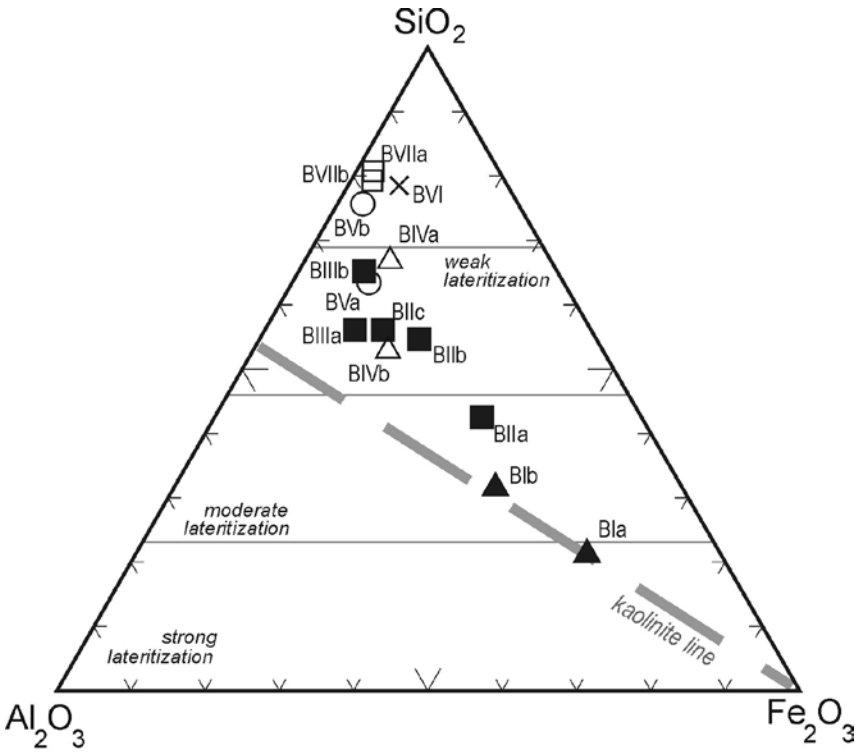
SiO2
BVIIa
BVIIb
BVI
BVb
BIVa
BIIIb
weak
lateritization
BVa
BIIc
BIIIa
BIIb
BIVb
BIIa
BIb
moderate
lateritization
BIa
kaolinite line
strong
lateritization
Al2O3
Fe2O3

Fig. 4

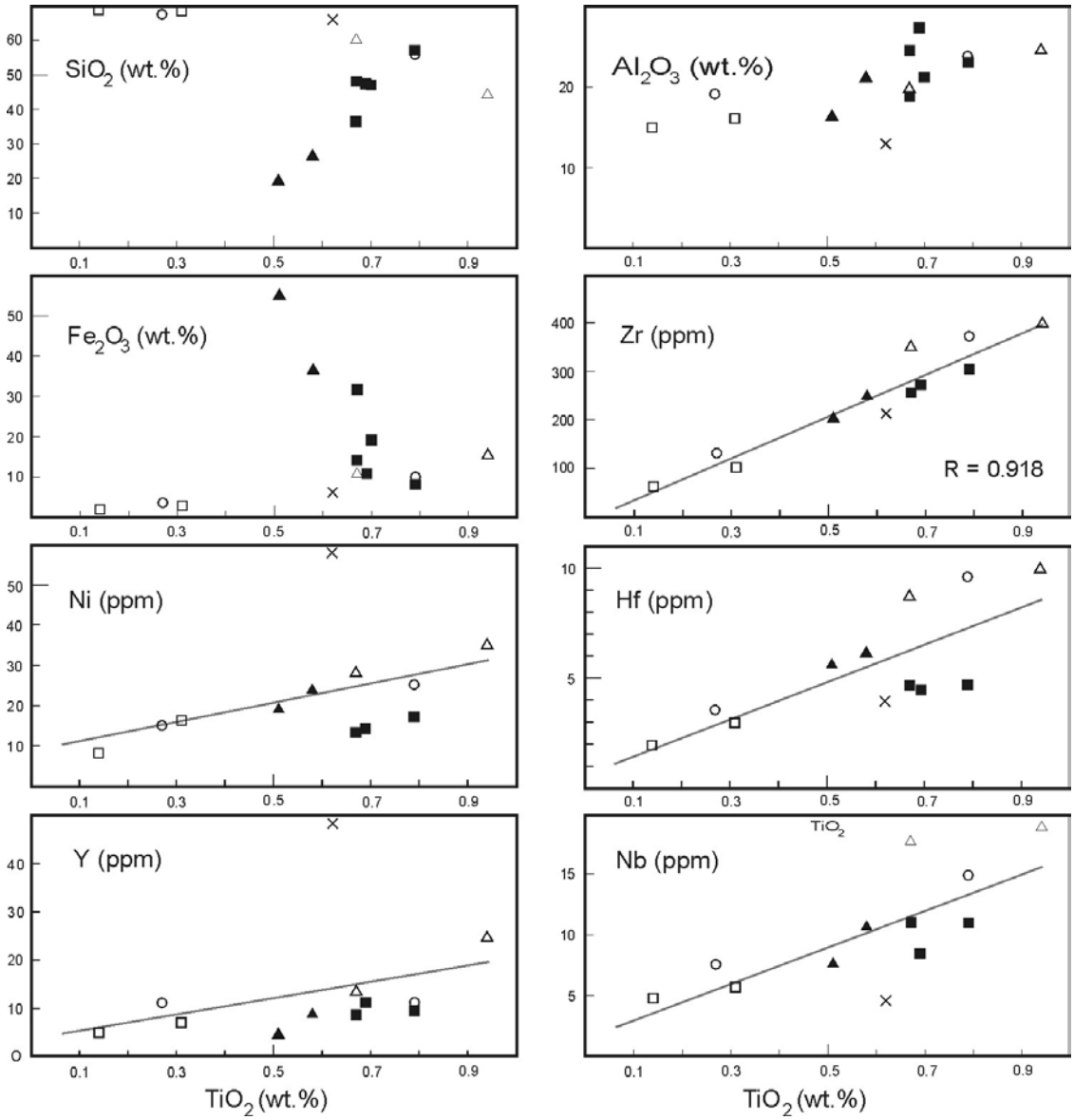
SiO2 (wt.%)
Al2O3 (wt.%)
Fe2O3 (wt.%)
Zr (ppm)
R = 0.918
Ni (ppm)
Hf (ppm)
Y (ppm)
Nb (ppm)
TiO2 (wt.%)
TiO2 (wt.%)

Fig. 5

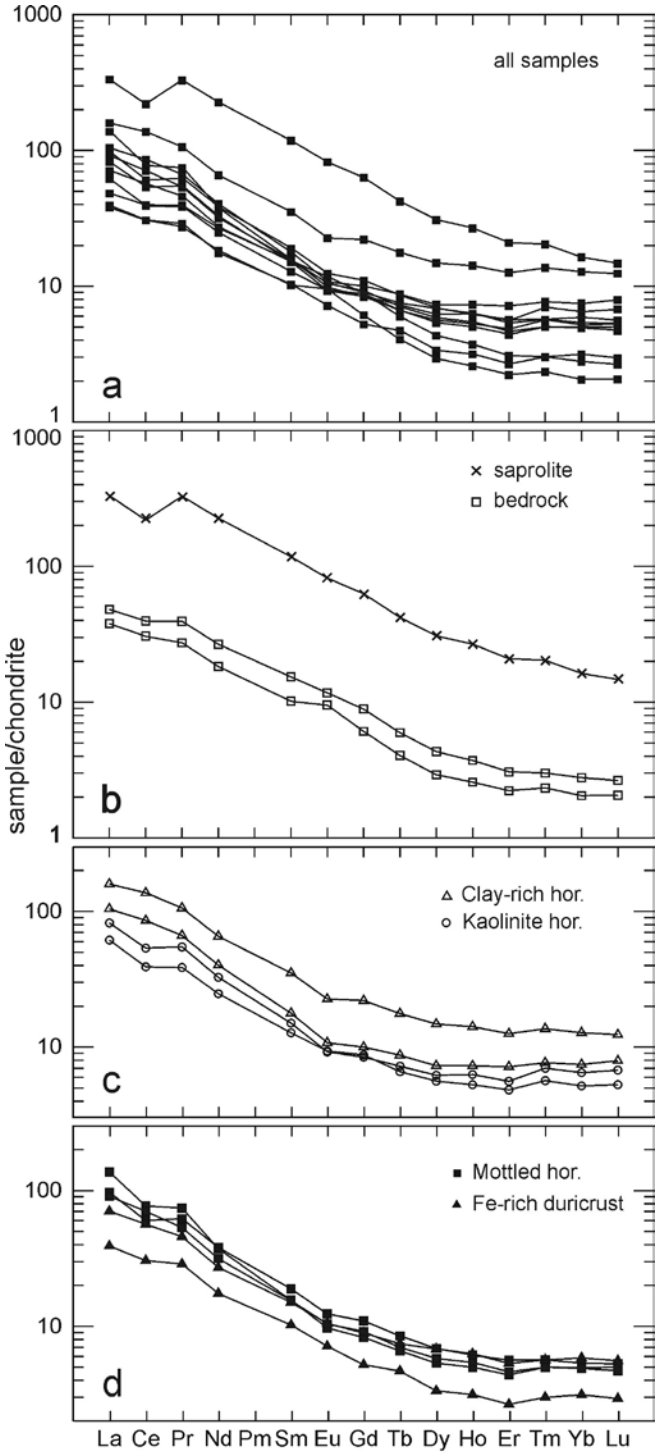
1000
100
10
1
all samples
a
saprolite
bedrock
b
sample/chondrite
Clay-rich hor.
Kaolinite hor.
c
Mottled hor.
Fe-rich duricrust
d
La Ce Pr Nd Pm Sm Eu Gd Tb Dy Ho Er Tm Yb Lu

Fig. 6

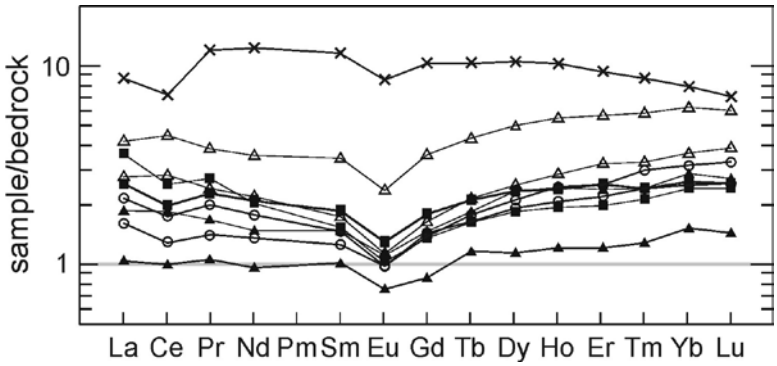
sample/bedrock
10
1
La Ce Pr Nd Pm Sm Eu Gd Tb Dy Ho Er Tm Yb Lu

Fig. 7

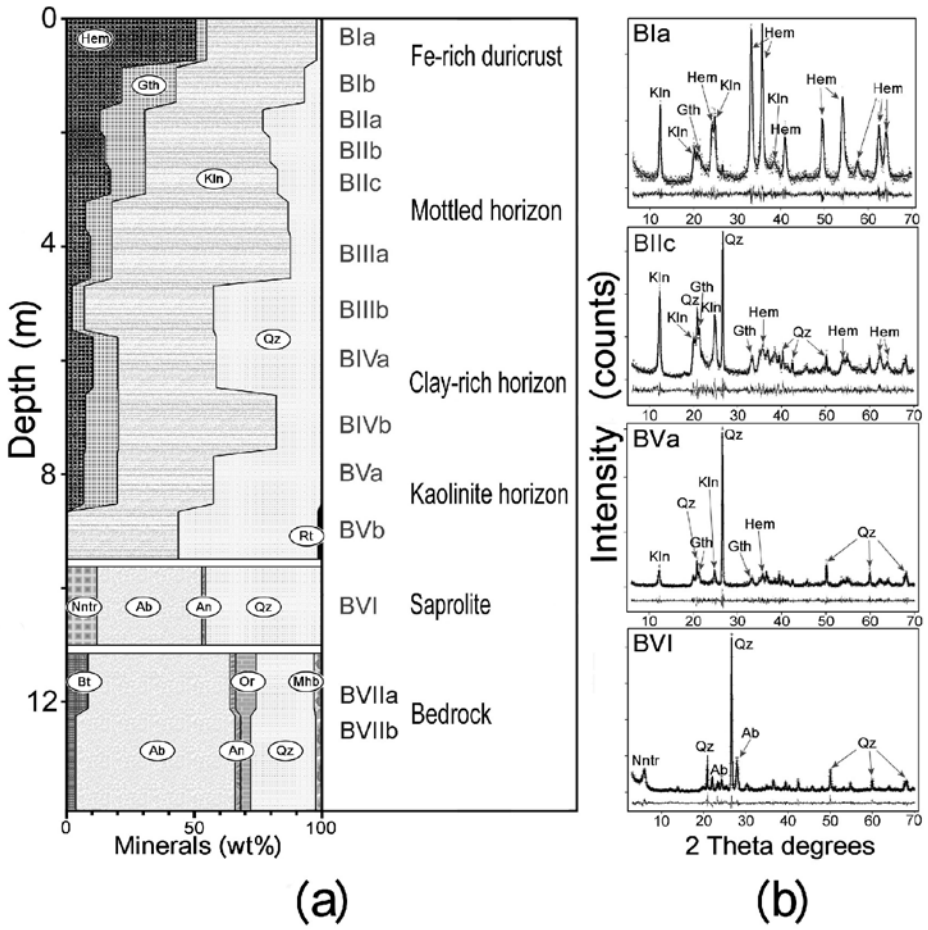
Depth (m)
0
4
8
12
Hem
Gth
Kln
Qz
Rt
Nntr
Ab
An
Bt
Or
Mhb
BIa
BIb
BIIa
BIIb
BIIc
BIIIa
BIIIb
BIVa
BIVb
BVa
BVb
BVI
BVIIa
BVIIb
Fe-rich duricrust
Mottled horizon
Clay-rich horizon
Kaolinite horizon
Saprolite
Bedrock
0
50
100
Minerals (wt%)
(a)
Intensity (counts)
BIa
BIIc
BVa
BVI
10 20 30 40 50 60 70
2 Theta degrees
(b)

Fig. 8

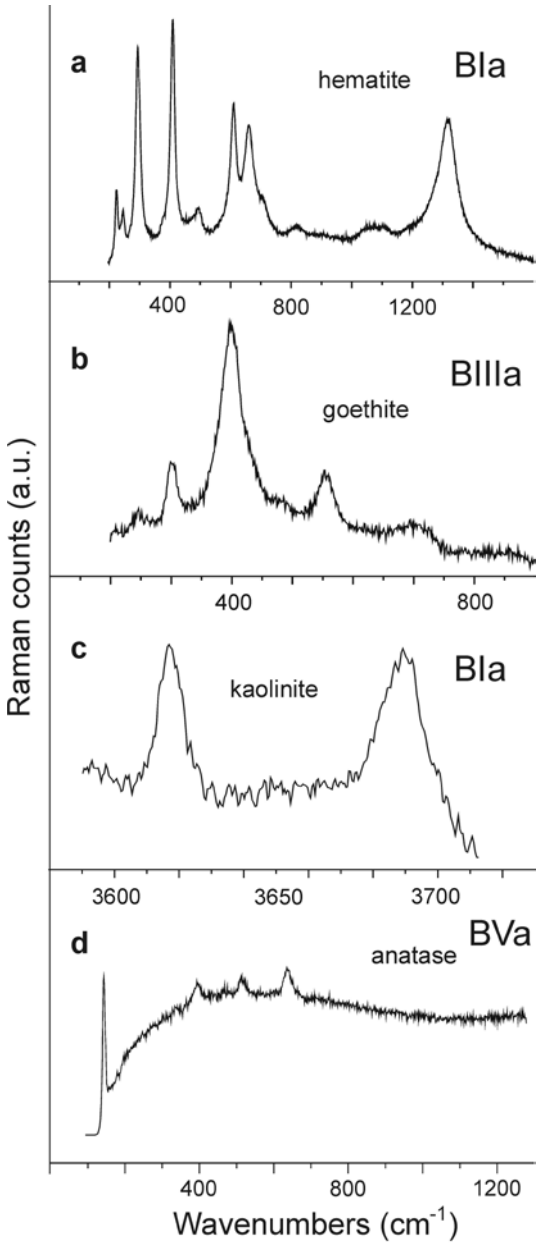
a
hematite
BIa
400
800
1200
b
BIIIa
goethite
400
800
c
kaolinite
BIa
3600
3650
3700
d
anatase
BVa
400
800
1200
Raman counts (a.u.)
Wavenumbers (cm-1)

Fig. 9

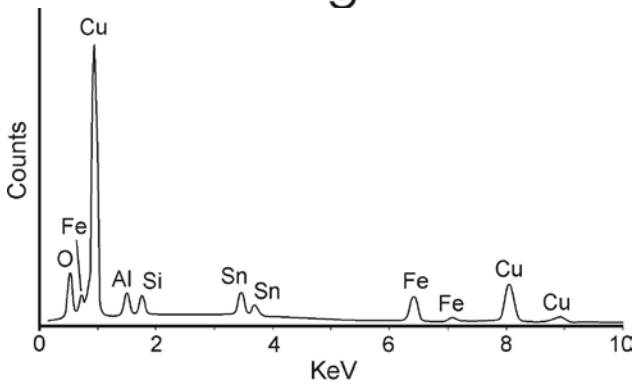
Cu
Fe
O
Al
Si
Sn
Sn
Fe
Fe
Cu
Cu
Counts
0
2
4
6
8
KeV

Fig. 10

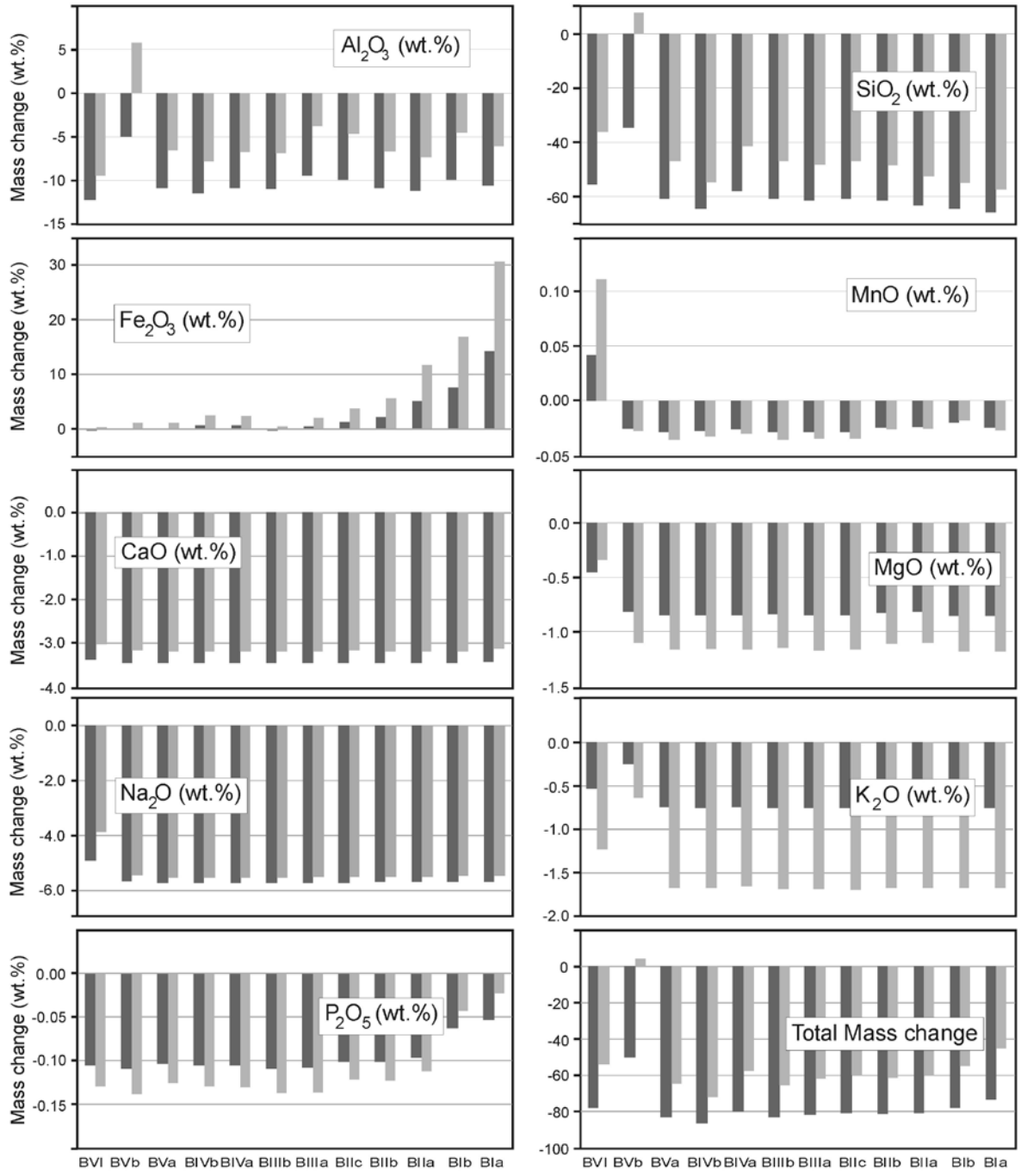
Mass change (wt.%)
Al2O3 (wt.%)
SiO2 (wt.%)
Fe2O3 (wt.%)
MnO (wt.%)
CaO (wt.%)
MgO (wt.%)
Na2O (wt.%)
K2O (wt.%)
P2O5 (wt.%)
Total Mass change
BVI BVb BVa BIVb BIVa BIIIb BIIIa BIIc BIIb BIIa BIb BIa

Fig. 11

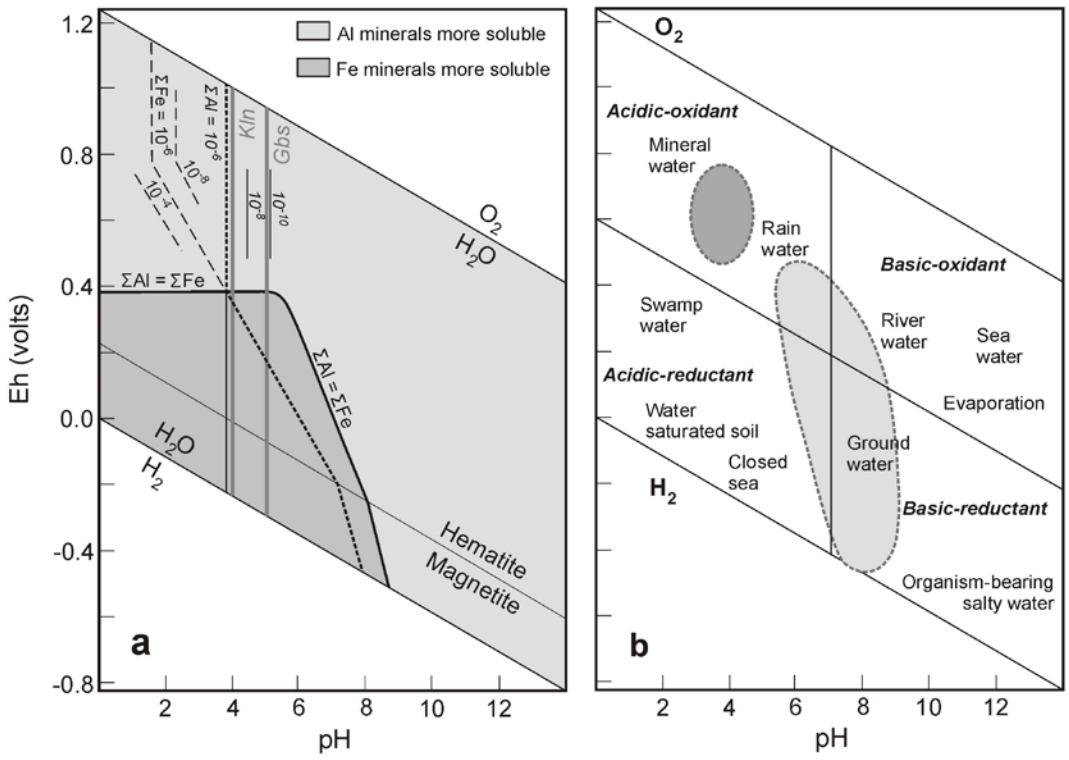
Al minerals more soluble
Fe minerals more soluble
ΣAl = 10⁻⁶
ΣFe = 10⁻⁶
10⁻⁸
10⁻⁴
Kln
Gbs
10⁻⁸
10⁻¹⁰
ΣAl = ΣFe
O2
H2O
H2O
H2
Hematite
Magnetite
a
Eh (volts)
pH
O2
Acidic-oxidant
Mineral water
Rain water
Basic-oxidant
Swamp water
River water
Sea water
Acidic-reductant
Evaporation
Water saturated soil
Ground water
Closed sea
H2
Basic-reductant
Organism-bearing salty water
b
pH

Fig. 12

Caption to Figures and Plate 1

Fig. 1. Geological sketch-map of the Balkouin area (from Castaing et al., 2003b), whose location is shown by the arrow within the inset. Legend: Birimian basement, rocks affected by the Eburnean metamorphism: 1: leptynite – granodiorite complex, 2: volcano-sedimentary schists, 3: amphibole gneiss, 4: rhyolite and rhyodacite. Birimian basement, intrusive magmatic rocks: 5: foliated granodiorite, tonalite and quartz-diorite (2140 ± 6 Ma), with quartz bodies (*q*), 6: biotite + amphibole porphyritic granodiorite, 7: biotite ± amphibole medium-grained granite, 8: biotite ± muscovite medium-fine grained granite, 9: pegmatite and aplite. Post-Birimian rocks: 10: dolerite dykes. Thick black lines are faults.

Fig. 2. Schematic representation of the whole Balkouin lateritic profile, from bottom (saprolite, which rests on the bedrock) to top Fe-rich duricrust. The stratigraphic position of the studied samples, described in detail in the text, is also shown.

Fig. 3. Chemical elements distribution vs. depth in the lateritic profile. Concentrations are given as wt % oxide for major elements and ppm for trace elements. Open symbols represent the bedrock contents. Dotted lines separate the main units (D: Fe-rich duricrust, M: mottled horizon, C: clay-rich horizon, K: kaolinite horizon, S: saprolite, B: bedrock).

Fig. 4. Al_2O_3-SiO_2-Fe_2O_3 (wt %) ternary diagram for the Balkouin lateritic profile. The fields of weak, moderate and strong lateritization, based on Schellmann (1983) classification and calculated from the Balkouin bedrock composition, are also shown. Symbols refer to the samples stratigraphic horizon. Black triangle: Fe-rich duricrust; black square: mottled horizon; open triangle: clay-rich horizon; open circle: kaolinite horizon; x: saprolite; open square: bedrock.

Fig. 5. Binary plots of selected major elements (wt %) and trace elements (ppm) against TiO_2 (wt %) (symbols as in Fig. 4). R: correlation coefficient (see discussion).

Fig. 6. Chondrite-normalized REE pattern for the studied profile. Chondrite-normalization values from Nakamura, 1974.

Fig. 7. Bedrock-normalized REE pattern for the Balkouin lateritic profile. Samples are normalized to specimen BVIIa (biotite ± amphibole granodiorite), considered as the most representative of the bedrock (see text). Symbols as in Fig. 4.

Fig. 8. (a) Main mineralogical composition, expressed as weight %, of the different horizons in the Balkouin lateritic profile, saprolite and bedrock. (b) Comparison, using the Rietveld method, between the experimentally collected (small crosses) and calculated (continuous line) X-ray diffraction patterns for selected Balkouin laterite specimens (BIa; BIIc; BVa; BVI), bearing indication of the main mineral phases [mineral abbreviations taken from Whitney and Evans (2010), except for Nontronite (Nntr)]. The flat profile of the related difference curves (almost straight lines below each diffraction pattern) certify the excellent fit between observed and calculated data, attesting reliability of the obtained quantitative estimates.

Fig. 9. Micro-Raman spectra of hematite, goethite, kaolinite and anatase in samples from the lateritic profile. In (d) the peaks diagnostic of anatase can be recognized, in spite of the strong background (due to the occurrence of some fluorescence in the sample). Mineral abbreviations according to Whitney and Evans (2010).

Fig. 10. Typical energy spectrum of the Cu-Sn phase (possibly a Cu-Sn intermetallic mineral: see text).

Fig. 11. Mass changes in the lateritic profile of Balkouin relative to the underlying bedrock. Calculations were performed relative to both samples BVIIa (dark grey bars) and BVIIb (light grey bars). The mass changes represent depletion or enrichment in wt %, or grams per 100 g, of the protolith.

Fig. 12. Eh-pH diagrams showing conditions relevant to the formation of laterite and bauxite. a: Eh-pH diagram showing the solubility relationships between hematite (or magnetite), gibbsite and water at T = 25°C and P = 1 atm (from Norton, 1973). The solubility contours of Fe and (in italics) Al are in moles/l. The heavy curve is the isosolubility curve ($\Sigma Al = \Sigma Fe$), which separates the fields where Al- (dark grey area) or Fe-phases (light grey area) are more soluble, respectively. Right of the dotted line neither Fe nor Al is mobile (solubility $\leq 10^{-6}$ moles/l; from Norton, 1973). The two thick vertical lines, dark grey in color, broadly correspond to the kaolinite-in (Kln) and gibbsite-in (Gbs) curves (from Dangic, 1985). b: Eh-pH diagram showing environments under atmospheric conditions (from Garrels and Christ, 1965) and the inferred conditions of formation of the Balkouin laterite (dark grey field), which are compared with those suggested for karstic bauxite from different localities (light grey: data from from Temur and Kansun, 2006; Zarasvandi, 2012; Liu et al., 2012, 2013).

Caption to Plate 1

Plate 1. Selected field photographs of the Balkouin lateritic profile. a: bedrock exposure, composed of granodiorite (BVIIa-BVIIb) crosscut by two generations of late magmatic dykes; b: saprolite (BVI); c-d: Kaolinite horizon, c: kaolinitic highly friable laterite (BVb), d: light red laterite (BVa); e: Clay-rich horizon, contact between the clay-rich laterite (BIVb) and the overlying “chaotic laterite” (BIVa); f-i: Mottled horizon, f: poorly coherent laterite (BIIIb), g: light reddish to whitish laterite (BIIIa), h: view of the Balkouin quarry, i: detail of the exposed face of the Balkouin quarry (BIIa-BIIb); l: upper part of the Fe-rich duricrust, displaying a pisolitic texture (BIa).

Table 1
Experimental methods adopted for the detailed characterization of the Balkouin lateritic profile (see also the Appendix).

Method	Purpose	Analytical details
X-ray Powder Diffraction (XRPD)	Qualitative identification of the main mineral phases in the rock. Quantitative ratios of main mineral components.	D-5000 Siemens, Bragg-Brentano diffractometer. Diffrac Plus (2005) evaluation package (EVA 11,00,3). GSAS program package for Rietveld method.
Micro Raman spectroscopy	Qualitative identification of minor/accessory mineral phases	LabRAM-HR 800 spectrometer equipped with a Nd solid state laser (532 nm, 100 mW).
SEM-EDS[1]	Spot chemical analyses for identification of minor/accessory mineral phases	SEM Cambridge Stereoscan 360- EDS Energy 200 and Pentafet Detector (Oxford Intruments). Data processed with INCA Suite v. 4.01
ICP-AES[2]	Whole rock analysis for identification of major elements	Detection limits: 0.01 wt.% oxide (ALS code: ME-ICP06 Chemex protocol)
ICP-MS[3]	Whole rock analysis for identification of minor and trace elements	Detection limits depending on the element (ALS code: ME-MS81 Chemex protocol)

[1] Scanning Electron Microscopy associated with Energy-Dispersive X-ray Spectroscopy
[2] Inductively Coupled Plasma-Atomic Emission Spectrometry
[3] Inductively Coupled Plasma-Mass Spectrometry

Table 2
Whole rock analyses of samples from the Balkouin lateritic profile and bedrock. *n.a.*: not analyzed.

Sample no.	BIa	BIb	BIIa	BIIb	BIIc	BIIIa	BIIIb	BIVa	BIVb	BVa	BVb	BVI	BVIIa	BVIIb
%														
SiO_2	19.05	26.42	36.12	46.84	47.80	47.05	56.69	60.34	44.22	56.11	67.64	65.88	68.91	69.70
TiO_2	0.51	0.58	0.67	0.70	0.67	0.69	0.79	0.67	0.94	0.79	0.27	0.62	0.14	0.31
Al_2O_3	16.25	21.10	18.67	21.07	24.40	27.20	23.00	19.85	24.50	23.6	19.05	12.9	14.80	16.00
Fe_2O_3	54.90	36.40	31.39	18.91	13.80	10.50	7.97	10.70	15.50	9.51	3.32	6.08	1.79	2.72
MnO	0.02	0.04	0.03	0.03	0.01	0.01	0.01	0.02	0.02	0.01	0.01	0.30	0.03	0.04
MgO	0.02	0.02	0.20	0.19	0.05	0.05	0.10	0.06	0.11	0.06	0.08	1.70	0.83	1.20
CaO	0.11	0.01	0.01	0.03	0.04	0.01	0.01	0.01	0.03	0.01	0.03	0.32	3.33	3.21
Na_2O	0.09	0.09	0.07	0.06	0.03	0.03	0.03	0.01	0.03	0.01	0.08	3.34	5.50	5.57
K_2O	0.08	0.10	0.11	0.12	0.07	0.08	0.10	0.14	0.14	0.13	0.95	0.98	0.74	1.73
P_2O_5	0.21	0.20	0.08	0.06	0.06	0.03	0.03	0.04	0.06	0.06	0.01	0.04	0.11	0.15
Cr_2O_3	0.10	0.10	0.08	0.04	0.03	0.03	0.03	0.02	0.06	0.02	0.01	0.02	0.01	0.01
LOI	9.77	13.70	10.90	11.15	12.25	12.75	11.05	10.00	12.75	10.70	8.16	7.35	0.80	0.83
Total	101.11	98.76	98.33	99.2	99.21	98.43	99.81	101.86	98.36	101.01	99.61	99.53	96.99	101.47
ppm														
Ni	19	24	*n.a.*	*n.a.*	13	14	17	28	35	25	15	58	16	8
Sr	15.5	16.9	*n.a.*	*n.a.*	22.6	21.7	17.3	25.4	28.2	17.9	57.3	120.5	1390	1260
Rb	2.4	3.7	*n.a.*	*n.a.*	2.9	2.8	3.8	9.7	10.9	6.5	28.3	21.4	12.7	43.6
Ba	18.8	26.5	*n.a.*	*n.a.*	24.9	43.5	26.7	44.6	60.7	37.1	447	1065	358	886
Zr	200	250	*n.a.*	*n.a.*	260	270	300	350	400	370	130	150	60	100
Hf	5.6	6.1	*n.a.*	*n.a.*	4.6	4.5	4.6	8.7	10.0	9.6	3.5	3.9	2.9	1.9
Nb	7.6	10.7	*n.a.*	*n.a.*	10.9	8.4	10.9	17.7	19.0	14.9	7.5	4.6	4.7	5.6
Y	4.6	8.9	*n.a.*	*n.a.*	8.4	11.0	9.3	13.5	24.8	10.9	11	48.4	4.7	6.8
La	12.9	23.3	*n.a.*	*n.a.*	45.3	32.1	30.0	34.4	52.5	27.1	20.3	109.5	12.5	15.9
Ce	26.4	49.0	*n.a.*	*n.a.*	66.8	52.2	61.0	74.1	118.5	46.4	33.8	189.5	26.4	34.2
Pr	3.22	5.12	*n.a.*	*n.a.*	8.33	6.96	5.97	7.43	11.85	6.13	4.32	36.8	3.06	4.41
Nd	11.0	17.1	*n.a.*	*n.a.*	23.5	24.0	19.9	25.3	41.3	20.6	15.6	142.5	11.5	16.8
Sm	2.08	3.05	*n.a.*	*n.a.*	3.17	3.84	3.15	3.61	7.14	3.05	2.59	23.9	2.06	3.11
Eu	0.55	0.81	*n.a.*	*n.a.*	0.75	0.95	0.8	0.83	1.74	0.71	0.72	6.31	0.73	0.9
Gd	1.44	2.47	*n.a.*	*n.a.*	2.29	3.03	2.53	2.76	6.08	2.33	2.42	17.35	1.68	2.45
Tb	0.22	0.35	*n.a.*	*n.a.*	0.31	0.4	0.33	0.41	0.83	0.34	0.31	1.98	0.19	0.28
Dy	1.15	2.34	*n.a.*	*n.a.*	1.84	2.36	1.99	2.5	5.07	2.13	1.93	10.55	1.0	1.48
Ho	0.22	0.44	*n.a.*	*n.a.*	0.35	0.43	0.38	0.51	0.99	0.44	0.37	1.87	0.18	0.26
Er	0.6	1.2	*n.a.*	*n.a.*	0.99	1.27	1.04	1.61	2.83	1.26	1.09	4.69	0.5	0.69
Tm	0.09	0.17	*n.a.*	*n.a.*	0.15	0.17	0.15	0.23	0.41	0.21	0.17	0.61	0.07	0.09
Yb	0.69	1.29	*n.a.*	*n.a.*	1.09	1.18	1.08	1.64	2.81	1.43	1.14	3.58	0.45	0.61
Lu	0.1	0.19	*n.a.*	*n.a.*	0.17	0.18	0.16	0.27	0.42	0.23	0.18	0.5	0.07	0.09
U	3.43	6.57	*n.a.*	*n.a.*	3.56	3.33	2.56	2.66	4.3	2.54	0.89	1.02	0.29	0.52
Th	19.85	11.75	*n.a.*	*n.a.*	7.65	10.35	5.92	8.47	11.00	8.47	3.28	1.85	1.76	1.65

Table 3
Mineralogical composition of the laterite horizons

Horizon	Major minerals (>10% vol.)	Minor minerals (1-10%)	Accessory minerals (<1%)
Fe-rich duricrust	hematite, kaolinite, goethite	quartz	Ti oxide[1], apatite
Mottled horizon	kaolinite, quartz, goethite	hematite	Ti oxide (rutile), apatite, Cu-Sn phase[2]
Clay-rich horizon	kaolinite, quartz, goethite	hematite	Ti oxide (anatase), apatite, Cu-Sn phase[2]
Kaolinite horizon	kaolinite, quartz, goethite	hematite	Ti oxide (rutile, anatase), zircon
Saprolite	quartz, albite, nontronite		Ti oxide
Bedrock	plagioclase, quartz	orthoclase, biotite, Mg-hornblende	titanite, zircon, apatite, rutile, epidote, allanite, Fe oxide(s)[3]

[1] 'Ti oxide' means that the recognition was done by SEM-EDS only; when further specification is given (such as 'rutile' or 'anatase'), the proper polymorph was identified by means of micro-Raman and/or XRPD techniques.
[2] see text.
[3] bedrock accessory phases from Castaing et al., 2003a.

Table 4
Quantitative mineralogical composition of the laterite horizons, saprolite and bedrock calculated with the Rietveld method (data expressed as wt%). Standard deviations are indicated in brackets.

		Balkouy lateritic profile (Burkina Faso)					
	Specimen	**Mineral phases**					
		Hematite	**Goethite**	**Kaolinite**	**Quartz**	**Rutile**	**Total**
Fe-rich duricrust	BIa	50.7(3)	4.1(3)	43.8(4)	1.4(1)	=	100.0 wt%
	BIb	21.1(3)	21.4(7)	50.2(4)	7.3(3)	=	100.0 wt%
	Average	35.9	12.8	47.0	4.4	=	100.1 wt%
Mottled horizon	BIIa	12.6(7)	17.7(5)	46.3(7)	23.4(7)	=	100.0 wt%
	BIIb	17.0(4)	14.0(5)	52.0(5)	17.0(3)	=	100.0 wt%
	BIIc	7.1(3)	10.1(7)	69.7(7)	13.0(4)	=	99.9 wt%
	BIIIa	8.8(5)	8.2(5)	70.6(3)	12.5(3)	=	100.1 wt%
	BIIIb	1.7(2)	4.2(2)	50.9(4)	43.1(3)	=	99.9 wt%
	Average	9.4	10.8	57.9	21.8	=	99.9 wt%
Clay-rich horizon	BIVa	10(2)	9.6(6)	39(1)	41.1(3)	=	99.7 wt%
	BIVb	7.1(6)	12.7(6)	62.2(8)	18.0(5)	=	100.0 wt%
	Average	8.7	11.1	50.6	29.6	=	100.0 wt%
Kaolinite horizon	BVa	6.0(6)	13(1)	38(1)	43.4(4)	=	100.4 wt%
	BVb	=	=	43.8(9)	55.2(3)	1.0(8)	100.0 wt%
	Average	3.0	6.5	40.9	49.3	0.5	100.2 wt%

		Nontronite	**Albite**	**Anorthite**	**Quartz**	**Total**
Saprolite	BVI	11.9(3)	41.2(5)	1(2)	46.1(4)	100.2 wt%

		Biotite	**Albite**	**Anorthite**	**Orthoclase**	**Quartz**	**Mg-Hornblende**	**Total**
Bedrock	BVIIa	3.8(3)	63.1(4)	1.9(3)	3.9(4)	25.6(3)	1.7(2)	100.0 wt%
	BVIIb	8.5(6)	55.9(4)	2.1(2)	7.8(4)	23.0(4)	2.7(4)	100.0 wt%
	Average	6.2	59.5	2.0	5.8	24.3	2.2	100.0 wt%

Table 5
Mass changes (MC) in the different horizons of the Balkouin lateritic profile. The changes are listed in weight percent, based on TiO_2 as the immobile component.

Sample no.	BVI	BVb	BVa	BIVb	BIVa	BIIIb	BIIIa	BIIc	BIIb	BIIa	BIb	BIa
SiO_2	-55.64	-34.66	-60.93	-64.60	-58.15	-60.88	-61.47	-60.94	-61.67	-63.59	-64.79	-66.06
TiO_2	0.62	0.27	0.79	0.94	0.67	0.79	0.69	0.67	0.70	0.67	0.00	0.00
Al_2O_3	-12.25	-4.97	-10.88	-11.48	-10.95	-11.02	-9.51	-9.92	-10.90	-11.22	-9.91	-10.62
Fe_2O_3	-0.38	-0.05	-0.05	0.61	0.53	-0.35	0.41	1.23	2.17	5.14	7.59	14.25
MnO	0.04	-0.03	-0.03	-0.03	-0.03	-0.03	-0.03	-0.03	-0.02	-0.02	-0.02	-0.03
MgO	-0.45	-0.82	-0.85	-0.85	-0.85	-0.84	-0.85	-0.85	-0.82	-0.82	-0.86	-0.86
CaO	-3.38	-3.45	-3.46	-3.46	-3.46	-3.46	-3.46	-3.45	-3.46	-3.46	-3.46	-3.43
Na_2O	-4.91	-5.67	-5.72	-5.71	-5.72	-5.71	-5.71	-5.71	-5.71	-5.70	-5.70	-5.69
K_2O	-0.53	-0.25	-0.74	-0.75	-0.74	-0.75	-0.75	-0.75	-0.74	-0.74	-0.74	-0.75
P_2O_5	-0.10	-0.11	-0.10	-0.10	-0.11	-0.11	-0.11	-0.10	-0.10	-0.10	-0.06	-0.05
Total MC	-77.61	-50.00	-82.76	-86.36	-79.45	-83.15	-81.48	-80.52	-81.25	-80.52	-77.94	-73.22